Bayesian galaxy shape measurement for weak lensing surveys - II. Application to simulations

T. D. Kitching, L. Miller, C. E. Heymans, L. van Waerbeke, A. F. Heavens

Mon. Not. R. Astron. Soc. **390,** 149–167 (2008) doi:10.1111/j.1365-2966.2008.13628.x

Bayesian galaxy shape measurement for weak lensing surveys – II. Application to simulations

T. D. Kitching,[1⋆] L. Miller,[1] C. E. Heymans,[2,3] L. van Waerbeke[2] and A. F. Heavens[4]

[1] *Department of Physics, Oxford University, Keble Road, Oxford OX1 3RH*
[2] *University of British Columbia, Department of Physics and Astronomy, 6224 Agricultural Road, Vancouver, BC, Canada V6T 1Z1*
[3] *Institut d'Astrophysique de Paris, UMR7095, CNRS, 98 bis bd Arago, 75014 Paris, France*
[4] *Scottish Universities Physics Alliance, Institute for Astronomy, University of Edinburgh, Royal Observatory, Blackford Hill, Edinburgh EH9 3HJ*

Accepted 2008 June 23. Received 2008 June 18; in original form 2008 February 11

ABSTRACT

In this paper, we extend the Bayesian model fitting shape measurement method presented in Miller et al., and use the method to estimate the shear from the Shear TEsting Programme simulations (STEP). The method uses a fast model fitting algorithm that uses realistic galaxy profiles and analytically marginalizes over the position and amplitude of the model by doing the model fitting in Fourier space. This is used to find the full posterior probability in ellipticity. The shear is then estimated in a Bayesian way from this posterior probability surface. The Bayesian estimation allows measurement bias arising from the presence of random noise to be removed. In this paper, we introduce an iterative algorithm that can be used to estimate the intrinsic ellipticity prior and show that this is accurate and stable.

We present results using the STEP parametrization that relates the input shear γ^T to the estimated shear γ^M by introducing a bias m and an offset c: $\gamma^M - \gamma^T = m\gamma^T + c$. The average number density of galaxies used in the STEP1 analysis was 9 per square arcminute, for STEP2 the number density was 30 per square arcminute. By using the method to estimate the shear from the STEP1 simulations we find the method to have a shear bias of $m = 0.006 \pm 0.005$ and a variation in shear offset with point spread function type of $\sigma_c = 0.0002$. Using the method to estimate the shear from the STEP2 simulations we find that the shear bias and offset are $m = 0.002 \pm 0.016$ and $c = -0.0007 \pm 0.0006$, respectively. In addition, we find that the bias and offset are stable to changes in the magnitude and size of the galaxies. Such biases should yield any cosmological constraints from future weak lensing surveys robust to systematic effects in shape measurement.

Finally, we present an alternative to the STEP parametrization by using a quality factor that relates the intrinsic shear variance in a simulation to the variance in shear that is measured and show that the method presented has an average of $Q \gtrsim 100$ which is at least a factor of 10 times better than other shape measurement methods.

Key words: gravitational lensing – methods: data analysis – methods: numerical – methods: statistical – cosmology: observation.

1 INTRODUCTION

It has been shown that weak lensing has the potential to become one of our most powerful cosmological probes (see Munshi et al. 2007 for a recent review of weak lensing; DETF, Albrecht et al. 2006; Peacock et al. 2006). By using redshift and weak lensing information, 3D weak lensing techniques have been developed that are particularly sensitive to the dark energy equation of state (for example, Heavens, Kitching & Taylor 2006; Taylor et al. 2007). Since the promise of weak lensing is now firmly established one must begin to focus on refining the technique and addressing systematic issues.

The determination of galaxy shape, and the inference of shear across an ensemble of galaxies for use in weak lensing is a challenging problem with a rich history. However recent studies of weak

⋆E-mail: tdk@astro.ox.ac.uk

lensing systematic effects (e.g. Amara & Refregier 2007; Kitching et al. 2008a) have shown that in order to fully utilize future weak lensing surveys (e.g. Pan-STARRS, Kaiser et al. 2002; SNAP, Kim et al. 2002; LSST, Tyson et al. 2003; DUNE, Refregier et al. 2006) in the determination of cosmological parameters, such as the equation of state of dark energy, the bias in the estimated shear as a result of any difference between a galaxy's true shape and the measured shape needs to be $\Delta e/e < 5\text{–}8 \times 10^{-3}$ (Amara & Refregier 2007; Kitching et al. 2008a). Currently-used methods, tested on simulations, have at best a 10^{-2} bias (Heymans et al. 2006; Massey et al. 2007b).

In this paper, we expand upon and apply to simulations the new shape measurement method LENSFIT[1] presented in Miller et al. (2007), a method which uses realistic galaxy profiles and fits these models to images using a fast fitting algorithm. The fast model fitting approach allows the entire posterior probability surface in ellipticity to be calculated. By including a prior the estimation of the shear can then be done in a fully Bayesian way. It was shown that a Bayesian estimator should be unbiased, given that realistic models and an accurate and correct intrinsic ellipticity prior are used. A new bias was discovered as a result of assuming that the prior is centred on zero-shear, that must be assumed given no knowledge of the intrinsic ellipticity distribution, but it was shown that this bias can be exactly corrected for to first order within the Bayesian formalism.

The simulations analysed in this paper are the publicly available simulations from Shear TEsting Programme (STEP).[2] The published STEP papers present the accuracy with which available shape measurement methods can recover the input shear from simulations of varying complexity. STEP1 (Heymans et al. 2006) used simulated galaxies that consist of a de Vaucouleurs bulge plus an exponential disc (in varying degrees), these are provided in sets of images with varying point spread functions (PSFs) and shear, there are 64 images covering five shear values for each of five different PSF types. In STEP2, Massey et al. (2007b) used shapelet generated galaxies and exponential galaxies, these are provided in sets of 128 images for each of six different PSFs.

In Miller et al. (2007), the results shown were for individual galaxy ellipticities, in this paper, we present results for shear. The results presented compare the estimated shear found using our technique with the known input shear of the simulations. Sections 2 and 3 review the shape measurement method, as well as extend the development by introducing a new way to determine the prior intrinsic ellipticity distribution from data. In Section 4, we describe the simulations in more detail and present the results from STEP1 and STEP2, respectively. We present a new way to characterize a shape measurement method's performance in Section 5. Discussion and conclusions will be presented in Section 6.

2 OVERVIEW OF LENSFIT

This section presents an overview of the LENSFIT shape measurement method, for an full description see Miller et al. (2007).

The method presented here combines two innovations in the shape measurement problem. First, the shear estimation is done in a fully *Bayesian* way, given a likelihood in ellipticity generated by some procedure and a prior on ellipticity it is possible to construct a shear estimator that is in principle unbiased. Secondly, we use *realistic* galaxy profiles to generate a full posterior probability surface in ellipticity.

The Bayesian shear estimation formalism can be applied to *any* shear measurement method that can produce a full likelihood surface in ellipticity. Similarly the fast model-fitting algorithm could be applied to any choice of model.

2.1 Overview of Bayesian galaxy shape measurement

For each galaxy a (Bayesian) posterior probability in ellipticity can be generated

$$p_i(\boldsymbol{e}|\boldsymbol{y}_i) = \frac{\mathcal{P}(\boldsymbol{e})\mathcal{L}(\boldsymbol{y}_i|\boldsymbol{e})}{\int \mathcal{P}(\boldsymbol{e})\mathcal{L}(\boldsymbol{y}_i|\boldsymbol{e})\mathrm{d}\boldsymbol{e}}, \tag{1}$$

where $\mathcal{P}(\boldsymbol{e})$ is the ellipticity prior probability distribution and $\mathcal{L}(\boldsymbol{y}_i|\boldsymbol{e})$ is the likelihood of obtaining the ith set of data values $\boldsymbol{y}_i$ given an intrinsic ellipticity $\boldsymbol{e}$.

We would hope that by considering the summation over the data the true distribution of intrinsic ellipticities can be obtained from the data

$$\left\langle \frac{1}{N}\sum_i p_i(\boldsymbol{e}|\boldsymbol{y}_i) \right\rangle = \int \mathrm{d}\boldsymbol{y} \frac{\mathcal{P}(\boldsymbol{e})\,\mathcal{L}(\boldsymbol{y}|\boldsymbol{e})}{\int \mathcal{P}(\boldsymbol{e})\,\mathcal{L}(\boldsymbol{y}|\boldsymbol{e})\,\mathrm{d}\boldsymbol{e}} \int f(\boldsymbol{e})\epsilon(\boldsymbol{y}|\boldsymbol{e})\mathrm{d}\boldsymbol{e}, \tag{2}$$

where $\epsilon(\boldsymbol{y}|\boldsymbol{e})$ is the probability distribution for the data $\boldsymbol{y}$ given an ellipticity $\boldsymbol{e}$ and $f(\boldsymbol{e})$ is the true (intrinsic) ellipticity distribution. On the right-hand side (RHS) we are integrating over the probability distributions to obtain the expectation value of the summed posterior probability distribution for the sample. This will be achieved under the conditions that $\epsilon(\boldsymbol{y}|\boldsymbol{e}) = \mathcal{L}(\boldsymbol{y}|\boldsymbol{e})$ and $\mathcal{P}(\boldsymbol{e}) = f(\boldsymbol{e})$ (assuming the likelihood is normalized, $\int \mathcal{L}(\boldsymbol{y}|\boldsymbol{e})\mathrm{d}\boldsymbol{y} = 1$) from which we obtain

$$\left\langle \frac{1}{N}\sum_i p_i(\boldsymbol{e}|\boldsymbol{y}) \right\rangle = \mathcal{P}(\boldsymbol{e}) = f(\boldsymbol{e}). \tag{3}$$

This is the equation that highlights the essence of the Bayesian shape measurement method, given a prior that matches the intrinsic distribution of ellipticities the estimated posterior probability should be unbiased. It may appear at first that having an accurate and correct measure of the prior distribution before estimating the ellipticity of galaxies may represent petitio principii, however this was partially addressed in Miller et al. (2007) and we extend and validate the issue of creating the prior in Section 3.

Throughout this paper we assume a galaxy's ellipticity $\boldsymbol{e}$ is defined by relating the axial ratio β and orientation ϕ of the galaxy via

$$\begin{pmatrix} e_1 \\ e_2 \end{pmatrix} = \frac{1-\beta}{1+\beta}\begin{pmatrix} \cos[2\phi] \\ \sin[2\phi] \end{pmatrix}. \tag{4}$$

The ellipticity can be related to the intrinsic galaxy ellipticity $\boldsymbol{e}^s$ in the weak lensing regime via:

$$\boldsymbol{e} = \frac{\boldsymbol{e}^s + \boldsymbol{g}}{1 + \boldsymbol{g}^\star \boldsymbol{e}^s} \tag{5}$$

from Seitz & Schneider (1997), where $\boldsymbol{e}$ is a complex variable and $\boldsymbol{g}, \boldsymbol{g}^\star$ are the reduced shear and its complex conjugate, respectively. The complex ellipticity is represented in terms of two components $\boldsymbol{e} = e_1 + ie_2$. In this formalism, we expect that $\langle \boldsymbol{e} \rangle = \boldsymbol{g}$ for an unbiased sample for which the average intrinsic ellipticity is zero, $\langle \boldsymbol{e}^s \rangle = 0$. As such we will use $\langle \boldsymbol{e} \rangle$ for a sample of galaxies as our estimator of shear $\boldsymbol{g}$. For a population of galaxies, we integrate over the

[1] For further information, and to download publicly available code, please go to http://www.physics.ox.ac.uk/lensfit

[2] http://www.physics.ubc.ca/~heymans/step.html

probability distribution in ellipticity, $f(\boldsymbol{e})$, to obtain the expectation value of ellipticity $\langle \boldsymbol{e} \rangle = \int \boldsymbol{e} f(\boldsymbol{e}) \mathrm{d}\boldsymbol{e}$. In the Bayesian formalism, we can write a similar expression for an individual galaxy if we know its Bayesian posterior probability distribution, and hence for a sample of N galaxies we can evaluate the sample mean as

$$\langle \boldsymbol{e} \rangle = \frac{1}{N} \sum_i \int \boldsymbol{e} p_i(\boldsymbol{e}|\,\boldsymbol{y}_i) \mathrm{d}\boldsymbol{e}. \tag{6}$$

This allows error estimates to be made on a galaxy-by-galaxy basis and each individual contribution to the signal to be evaluated.

In measuring shear we cannot know in advance the correct prior to apply, even if we know the intrinsic unsheared ellipticity prior probability distribution, because the amount of shear varies over the sky in a way that we are attempting to measure. We must therefore use a prior that contains zero shear. The result of having a zero-shear prior introduces the need to add a weight to the ellipticities to counter the effect of this assumption. This *shear sensitivity* is an effect that has been identified by a number of shape measurement methods, for example Bernstein & Jarvis (2002), Luppino & Kaiser (1997), Kaiser (2000) and Massey et al. (2007a) (it has also been called shear 'polarizability' or 'responsivity'). Crucially the Bayesian methodology allows the magnitude of this effect to evaluated on a galaxy-by-galaxy basis directly from the data.

The shear sensitivity for an individual galaxy may be quantified as $|\partial \langle \boldsymbol{e} \rangle_i / \partial \boldsymbol{g}|$: a measure of how the measured mean ellipticity $\langle \boldsymbol{e} \rangle_i$ for the ith galaxy depends on the shear $\boldsymbol{g}$. For measurements on noisy data we expect the sensitivity to be reduced from the ideal value of unity. For a given sample of N galaxies the estimator of the shear is now given by

$$\hat{\boldsymbol{g}} = \frac{\sum_i^N \langle \boldsymbol{e} \rangle_i}{\sum_i^N |\partial \langle \boldsymbol{e} \rangle_i / \partial \boldsymbol{g}|}. \tag{7}$$

This is the key equation used to estimate the shear. The shear sensitivity for an individual galaxy falls within in the range $0 < \partial \langle \boldsymbol{e} \rangle_i / \partial \boldsymbol{g} \leq 1$, for a measurement completely dominated by noise $\partial \langle \boldsymbol{e} \rangle_i / \partial \boldsymbol{g} \sim 0$.

The shear sensitivity can be calculated to first-order using the likelihood and the prior probability distributions for an individual galaxy using

$$\frac{\partial \langle \boldsymbol{e} \rangle}{\partial \boldsymbol{g}} \simeq 1 - \frac{\int (\langle \boldsymbol{e} \rangle - \boldsymbol{e})\, \mathcal{L}(\boldsymbol{e}) \dfrac{\partial \mathcal{P}}{\partial \boldsymbol{e}} \mathrm{d}\boldsymbol{e}}{\int \mathcal{P}(\boldsymbol{e}) \mathcal{L}(\boldsymbol{e}) \mathrm{d}\boldsymbol{e}}. \tag{8}$$

In the case that $\mathcal{P}(\boldsymbol{e})$ is fitted with a function, $\frac{\partial \mathcal{P}}{\partial \boldsymbol{e}}$ can be evaluated analytically.

The summation over the posterior probabilities, used here to find the mean ellipticity and hence shear of a sample, could be replaced by a convolution of all the posterior probability distributions. For a set of N galaxies with mean ellipticity $\langle \boldsymbol{e} \rangle$, this would yield the probability distribution $P(N\langle \boldsymbol{e} \rangle)$ whose expectation value is given by N times the mean, that we calculate here by summation. This would be a useful procedure for making weak-lensing maps. For cosmological studies, we may be more interested in quantities such as shear variance or the shear power spectrum, for which the calculation of a full posterior probability distribution is less straightforward. We leave a full discussion of this issue for a future publication.

Alternatively, the LENSFIT method can be used in exactly the same way as any traditional shape measurement method. For example a shear estimator can be calculated on a galaxy-by-galaxy basis from the posterior probability distribution, and the shear variance, E and B modes and shear power spectrum can then be calculated using standard procedures.

2.2 Overview of fast realistic galaxy model fitting

The method we use to evaluate the likelihood of a galaxy's ellipticity $\mathcal{L}(\boldsymbol{e})$ is to fit a model surface brightness profile to each galaxy image (earlier shape measurement methods that use model fitting are presented in Bridle et al. 2002; Kuijken 1999). For a simple model galaxy whose profile is parametrized by a characteristic radius the total number of free parameters that need to be estimated is six: position (two parameters), ellipticity (two parameters), brightness and the radius. The key innovation of the work presented in Miller et al. (2007) is that if the model fitting is done in Fourier space then the marginalization over position and brightness can be done analytically, therefore speeding up the model estimation, leaving only the radius to be marginalized over to obtain the ellipticity likelihood $\mathcal{L}(\boldsymbol{e})$. By using fast Fourier transform techniques the method can provide a full likelihood surface for an individual galaxy in $\sim$1 s (on a standard 2 GHz CPU).

As shown in Miller et al. (2007) the likelihood of a model galaxy being the correct fit to a galaxy image can be written as

$$\mathcal{L} \sim \sqrt{\frac{2\pi}{A}} \mathrm{e}^{-\sum y_i^2 / 2\sigma_i^2} \mathrm{e}^{AB^2/2}. \tag{9}$$

This has been analytically marginalized over the amplitude of the model, A and B are summations over combinations of the data y_i and model y_i^m defined in Miller et al. (2007) and σ_i is the statistical uncertainty of the data.

To marginalize over position it is more straightforward to work in Fourier space, where the data and model vectors can be rewritten as

$$y_i = \sum_k y_k \mathrm{e}^{-i\boldsymbol{k}.\boldsymbol{x}_i} \qquad \text{and} \qquad y_i^m = \sum_k y_k^m \mathrm{e}^{-i\boldsymbol{k}.\boldsymbol{x}_i}. \tag{10}$$

One can simplify the various summations by assuming that faint galaxies are being used in weak lensing measurement, such that σ_i is dominated by the background photon shot noise and is constant for all pixels. This assumption of spatially invariant noise is applicable to faint galaxies but not for very bright galaxies, but since weak lensing is concerned with faint galaxies this assumption is valid. To take into account the effect of position uncertainty a shift $\boldsymbol{X}$ is introduced into the model position, so that the new model becomes

$$y_i^{m\prime} = \sum_k y_k^m \mathrm{e}^{-i\boldsymbol{k}.\boldsymbol{x}_i} \mathrm{e}^{-i\boldsymbol{k}.\boldsymbol{X}}. \tag{11}$$

Substituting into equation (9) the likelihood becomes

$$\mathcal{L} \propto \exp\left[\frac{|h(\boldsymbol{X})|^2}{2\sigma^2 \sum y_i^{m\,2}}\right], \tag{12}$$

where $h(\boldsymbol{X})$ is the cross-correlation of the data y_i with the model y_i^m. To marginalize over $\boldsymbol{X}$ Miller et al. (2007) adopt a prior on position chosen to be a Gaussian centred on some previously estimated position and that falls off to zero at large distances.

If the cross-correlation function has the Gaussian form $h = h_0 \exp[-(r - r_0)^2/s^2]$ and we approximate the likelihood itself as a Gaussian, then it can be shown that the likelihood, now marginalized over position and amplitude, becomes

$$\mathcal{L} \propto \frac{\pi s^2}{2b^2} \frac{e^\beta}{\beta} \mathrm{e}^{-r_0^2/2b^2}, \tag{13}$$

where β depends on the amplitude of the cross-correlation (see Miller et al. 2007), r_0 is the nominal galaxy position, s is the variance of the cross-correlation and b is the prior uncertainty on the galaxy position. This is another key equation which is used in the LENSFIT implementation, that is, if the width s, amplitude h_0 and centroid

r_0 of the cross-correlation function can be determined then the marginalized likelihood may be estimated from equation (13).

For our model we choose an exponential profile which has been shown to be a good estimate of realistic galaxy profiles. For faint galaxies, exponential and de Vaucouleurs profiles are indistinguishable. The STEP simulations present a real challenge of this choice since STEP1 consists of composite exponential+de Vaucouleurs profiles and STEP2 uses complex galaxy morphologies. To create a sheared set of galaxy models the axial ratio β and orientation of the model ϕ are related to ellipticity using equation (4). So in the case of an exponential profile, equation (13) yields a likelihood as a function of e_1, e_2 and the scale radius of the model $\mathcal{L}(e_1, e_2, r)$. To obtain the likelihood as a function of ellipticity, so that it can be used in equation (7), we analytically marginalize over the radius using a simple summation

$$\mathcal{L}(e_1, e_2) = \int \mathrm{d}r \mathcal{L}(e_1, e_2, r) \approx \sum_{r_{\min}}^{r_{\max}} \mathcal{L}(e_1, e_2, r) \Delta r, \qquad (14)$$

where $r_{\min}$ and $r_{\max}$ are some minimum and maximum that are numerically justified in the following Section 2.3.

2.3 Numerical range and resolution

Here we show how the resolution and range in the model parameter variables are chosen. We choose a grid in e_1, e_2 and r to search the parameter space, however this is not essential and one could imagine using a Monte Carlo Markov Chain (MCMC) if this was preferable in terms of speed or accuracy. The level of accuracy with which the parameter space needs to be characterized, and hence the range and resolution of the parameters needed, depends on the data set used, and particularly on the signal-to-noise ratio of the galaxies. For example, in the case that the likelihood surfaces are sharp delta functions, the parameter space may need to have a finer sampling than if the likelihood surfaces are broad. Since weak lensing surveys target faint galaxies, the likelihood surfaces should dominantly be broad so that a finite grid sampling should be the fastest method.

The only numerical parameters that need to be specified are, in the case of a grid search in (e_1, e_2, r), the resolution in ellipticity Δe and the range and resolution in the scale factor $r_{\min}$, $r_{\max}$ and Δr. Fig. 1 shows the values of the parameters that are used in Bayesian shear estimation ($\langle e \rangle$, $\langle e^2 \rangle$ and $\partial \langle e_i \rangle / \partial g_i$), measured from the LENSFIT code, for various values of the model parameter's range and resolution. To ensure that the code is numerically stable we use values of $\Delta e = 0.1$, $\Delta r = 0.2$ pixels and $r_{\max} = 10$ pixels throughout the remainder of this paper. For $r_{\max}$ and Δr, these values are well within the numerically stable regime. We choose these values so that the code is assured to be robust, when marginalizing over the radius, as a result of this built-in redundancy. Some additional redundancy could be built-in at the expense of computational time; the time to find the full posterior likelihood scales as $1/\Delta e^2$. We set the minimum radius investigated to $r_{\min} = 0$, any objects for which the most likely value is $r \equiv 0$ we identify as stars and do not use in the average shear estimation. The values of Δe, Δr and $r_{\max}$ imply that our 3D parameter space in (e_1, e_2, r) has less than $20 \times 20 \times 50$ points for which the likelihood must be evaluated. This is much less than the number of MCMC evaluations that would need to be performed in order to fully characterize the three dimensional (e_1, e_2, r) parameter space.

We also present an investigation into the marginalization over the position of the centroid of the galaxy. The results from LENSFIT should be robust to inaccuracies in the centroid position of any galaxy, since the method analytically marginalizes over galaxy position uncertainty (Miller et al. 2007). In Fig. 1, we introduce a constant offset in the position of every galaxy from the actual galaxy position. It can be seen that the method is relatively insensitive up to a constant offset of $\sim$10 pixels so that when estimating the position of galaxies any source extraction routine could misplace galaxies by up to this amount with no major effect on the shear estimation (this result was also presented in Miller et al. 2007; here we additionally show Fig. 1). In reality source extraction routines such as SExtractor (Bertin & Arnouts 1996) or HFINDPEAKS (part of the IMCAT[3] software package) have accuracies much better than this (Heymans et al. 2006).

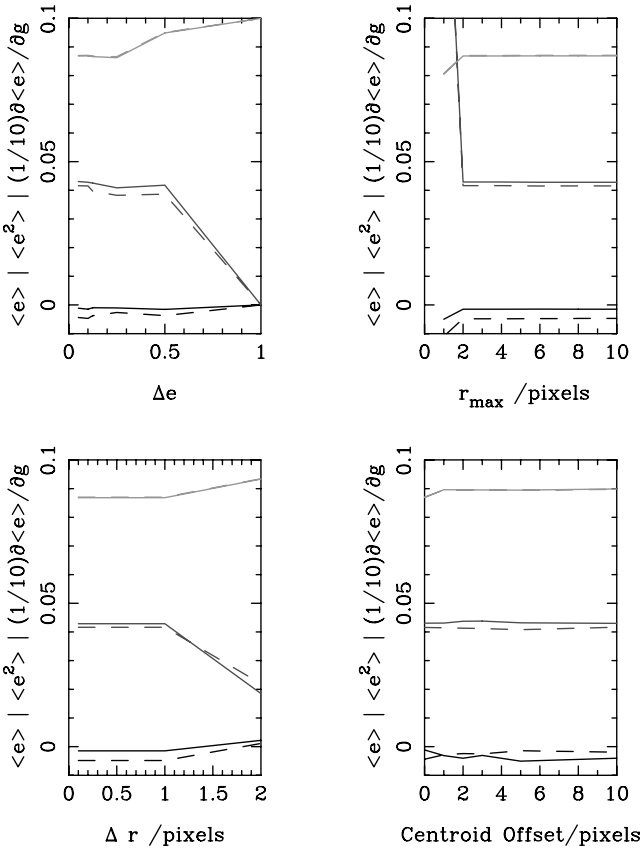

Figure 1. Variation in the expectation value of the ellipticity $\langle e_i \rangle$ (black, lowest lines), the variance in ellipticity $\langle e_i^2 \rangle$ (green, middle lines) and the shear sensitivity $\mathrm{d}e_i/\mathrm{d}g_i$ (red, upper lines) for γ_1 (solid lines) and γ_2 (dashed lines) as a function of the model parameter values used in the LENSFIT code. The y-axis' displays the value of each of these quantities $\langle e_i \rangle$, $\langle e_i^2 \rangle$ and $\partial \langle e_i \rangle / \partial g_i$ individually; we scale the sensitivity by 1/10 to fit the values within the y-axis range. The top left-hand panel shows the result of changing the resolution in ellipticity Δe. The top right- and bottom left-hand panels show the result of changing the range $r_{\max}$ and the resolution Δr of the model galaxy radius. As each model parameter is varied the others are kept at the values of $\Delta e = 0.1$, $\Delta r = 0.2$ pixels and $r_{\max} = 10$ pixels, which are the values that we use in the remainder of the paper. The lower right-hand panel shows how $\langle e_i \rangle$, $\langle e_i^2 \rangle$ and $\partial \langle e_i \rangle / \partial g_i$ vary as the nominal catalogue position of every galaxy is offset. This tests the ability of the method to marginalize over the position of the galaxy centroid. The simulation used was the STEP1 PSF 0 zero-shear image, the results are for the average over the whole galaxy ensemble.

[3] www.ifa.hawaii.edu/~kaiser/imcat/content.html

In the implementation of the method we extract a small postage-stamp image about each galaxy. This postage stamp size then determines the size of the model and PSF. We use a postage stamp size of 32×32 pixels, that is the same for the model, PSF and galaxy images. We reject any galaxies that are in a close pair, that is, ones which have one or more other galaxies within their postage stamp. It is possible to intelligently reject close galaxy pairs based on signal-to-noise criterion, for example, Schrabback et al. (2007) and Leauthaud et al. (2007) employ more sophisticated close-pair rejection algorithms, however we have not implemented this technique here. The postage stamp size was optimized for the STEP simulations; if the postage stamp size is too large then too many galaxies will have 'close neighbours' (i.e. another galaxy or star in the postage stamp) and be rejected, if too small then the largest galaxies will not fit into the postage stamp. We found that a 32×32 stamp was the smallest stamp in which every galaxy could fit,[4] allowing for the postage stamps to be a factor of 2 larger to minimize edge effects. We create a model galaxy on a grid the size of the postage stamp and fit this model to the data, hence an edge effect could occur if the surface brightness profile of the galaxy is artificially truncated at the postage stamp's edge. In principle the LENSFIT technique could model this truncation by creating a galaxy model on a large grid and truncating the model. We did not find that such a sophistication was necessary. An adaptive postage stamp size could be used to minimize the number of close pairs, that is, a smaller postage stamp for smaller galaxy images, though we leave this sophistication for future work.

The size of the postage stamp does not determine $r_{\rm max}$, and as we have shown a value $r_{\rm max} = 10$ pixel is sufficient to ensure numerical accuracy.

2.4 Pixelization and PSF estimation

The level of accuracy with which a PSF can be characterized is an important factor in the performance of any shape measurement method. As described by Massey et al. (2007b), the PSF must either be deconvolved from the image to generate a raw galaxy image or, more robustly, in LENSFIT a galaxy model is convolved with the PSF and then fitted to the data. Existing methods usually either stack star images or fit functional forms to star images. A limitation of all methods is that the spatial and chronological variability of the PSF needs to be determined, for which only a finite number of stars in each image are available (e.g. Paulin-Henriksson et al. 2008).

We create the PSF model by stacking star images selected using the SExtractor 'class_star' parameter. The data for each star are subsampled on to a 50 times finer pixel grid using sinc function interpolation (that precisely preserves the data values without inventing any new Fourier modes), and stacking takes place in a two-stage iterative process. In the first stage, the stars are co-aligned by cross-correlating with a delta function, and then co-added. Then, each star is individually compared with the stack by cross-correlation, any that have a low cross-correlation amplitude are rejected. In the second stage, the remaining stars are again cross-correlated with the stacked PSF to redetermine their centroids more accurately, the stack is remade and again individual stars are checked by cross-correlation with the new stack, and eliminated if appropriate. The stack of surviving stars thus forms the final PSF that is then down-sampled to the original pixel sampling (without aliasing since in the above process there have been no modes created above the Nyquist frequency). We find in the STEP simulations that if stars of low signal-to-noise ratio are used, many are rejected at the cross-correlation stage. Stars with peak signal-to-noise ratio greater than 30 worked well, with only a small number of stars being rejected, these being instances of closely neighbouring stars being blended together. No selection of stars 'by eye' was required.

In generating the PSF-convolved models, the method described takes full account of the effect of pixelization in the case of fully-sampled data. Models are generated that are sampled on a grid which is finer than the data pixel sampling by a factor of 4 (the value of this oversampling factor makes little difference to the measured galaxy ellipticities) and are then transformed to the Fourier domain ready for the convolution step. The PSFs generated as described above represent the combined effects of atmospheric, telescope and detector pixel PSFs, and this total PSF is sampled with the data pixel sampling. Thus when the models are convolved with the PSF the data pixelization is included in the resulting convolved model.

If the true PSF is band-limited at the pixel sampling Nyquist frequency the above method produces a faithful representation of it in the sampled image plane. Convolution with a galaxy model then yields an 'observational model' of the galaxy with the effects of the PSF and pixel sampling correctly matched to the data. In reality, the band-limited assumption is not likely to be true, and all methods of PSF determination and hence galaxy shape measurement are ultimately limited by the problem of pixelization: we have no information on the PSF below the pixel scale, and any Fourier modes in the PSF with frequencies higher than the Nyquist frequency become aliased to lower measured frequencies. There is, in principle, some information available on the subpixel scale owing to the centres of the stars not being exactly centred on pixels, but in reality it is very hard to extract that information to yield a robust estimate of the high frequency modes in the presence of noise. Without such information the best we can do is to assume that the sampling of the PSF is sufficient to render aliasing of high frequency modes insignificant. This deficiency of information may become one of the main limiting factors in the accuracy with which weak lensing shear may be measured. Dithering of images would also allow us to gain back information on the subpixel scale and for some future space-based experiments such as DUNE or SNAP, high-resolution pre-launch characterization of the PSF should allow improved PSFs to be reconstructed. Jarvis & Jain (2005) and Jee et al. (2008) discuss the characterization of a PSF using PCA techniques which can be used for ground-based surveys.

3 ESTIMATION OF THE PRIOR

A requirement of the Bayesian shape measurement approach is the accurate and correct estimation of the ellipticity prior. Here, we present an iterative method that should yield the correct prior from the data itself (this is similar to the approach introduced in Lucy 1974; Richardson 1972 and Lucy 1994 in image deconvolution). One could use the entire data set or a subset of a large wide field survey to do this. Many planned future surveys, for example DUNE, Pan-STARRS, SNAP and LSST include in their strategies medium-deep surveys over much smaller areas than the main wide field surveys which would be used for cosmic shear analysis. These medium-deep surveys would be ideal data sets from which to estimate the prior.

[4] The fast Fourier transforms techniques which are used by LENSFIT work fastest for grid sizes that have a number of pixels which are power of 2. However, the gain in computational speed by choosing a power of 2, over another number, is not a dominating factor in the total computational time used.

As already discussed in Miller et al. (2007) one must assume a prior with zero shear, that is, centred on $e_1 = e_2 = 0$, since this is a baseline assumption that enforces no a priori knowledge on the result. The level of bias introduced by this assumption can be exactly accounted for within the Bayesian formalism by using the shear sensitivity, equation (7). Also, in the case of real data one would expect the shear to average to zero over a sufficiently large number of galaxies. In the STEP simulations there can be a large shear ($\gamma \sim 0.10$ in STEP1 and $\gamma \sim 0.06$ in STEP2) over a whole image which in reality one would not expect, and the simulations thus test this assumption of a zero-centred prior to an extreme. When testing on simulations the prior has to be found using a zero-shear image since the posterior probability estimated from these images will be the intrinsic ellipticity distribution, however in a real data set where the mean shear across an image should be zero the prior can be estimated directly from the data.

The iterative approach centres around equation (3) which is the average summed posterior probability for an ensemble of N galaxies

$$\left\langle \frac{1}{N} \sum_{\alpha} \frac{\mathcal{P}(\boldsymbol{e})\mathcal{L}(\boldsymbol{e})_{\alpha}}{\sum_{\boldsymbol{e}} \mathcal{P}(\boldsymbol{e})\mathcal{L}(\boldsymbol{e})_{\alpha}} \right\rangle = \mathcal{P}(\boldsymbol{e}), \tag{15}$$

where for each galaxy the posterior probability is normalized. If the prior initially used were the true, intrinsic, prior this would be a stable equation provided that a sufficient number of galaxies are used, that is, if the prior that is output on the RHS of the equation is used on the left-hand side (LHS) of the equation in a second iteration the result will be the same. If the prior used on the LHS is not the true prior then the distribution given on the RHS will be closer to the true intrinsic distribution than the prior initially used. The method involves using this equation to iterate on the prior, i.e.

$$\mathcal{P}(\boldsymbol{e})_{i+1} = \left\langle \frac{1}{N} \sum_{\alpha} \frac{\mathcal{P}_i(\boldsymbol{e})\mathcal{L}(\boldsymbol{e})_{\alpha}}{\sum_{\boldsymbol{e}} \mathcal{P}_i(\boldsymbol{e})\mathcal{L}(\boldsymbol{e})_{\alpha}} \right\rangle. \tag{16}$$

This is repeated over i iterations, when the prior used is an accurate and correct representation of the true intrinsic prior a stable solution will have been found. This iterative approach, and the method in general, assumes that the function that is used as the prior is continuous and non-zero at all points in the parameter space at which the likelihood is evaluated.

One may be concerned that iterating on data would lead to divergent results; for example if data were used to estimate the likelihood of a parameter and that likelihood were used as the prior in a second iteration then the result could diverge. Crucially, this common concern involved with iterating on a data set does not apply here. This is due to the nature of the operation: we are not using a prior to improve the probability distribution of some estimated parameter, but rather use the data to estimate the prior. Since the operation described above yields the prior itself once the true prior is found this operation could be performed given a sufficient number of galaxies {ad infinitum} with no divergence of results. In the limit of a small number of galaxies, this stability will diverge owing to shot noise (i.e. sampling variance) in ellipticity, in Section 3.2 we estimate the minimum sample sizes that are needed for convergence to a correct prior.

3.1 Fitting the prior

In practice after each iteration we fit the prior surface with a functional form and use this as the prior for the next iteration. This is done since a functional form ensures that the prior is known everywhere, also using a functional form means that the derivative of the prior, to use in equation (8) can be calculated exactly. To avoid divergence we do not allow the functional form to have turning points in the region $0 < |e| < 1$, if turning points were admitted then in an iteration such structures could become artificially amplified. This assumption should be valid in reality since there is no a priori reason to expect a particular non-zero intrinsic ellipticity to be preferred (or disfavoured) by a large ensemble of galaxies. The fitting of this simple functional form results in a 'smoothed' representation of the prior, that is, any small-scale structure and noise has been averaged over. The requirements on the fitted functional form ensure that no stopping criterion is needed, since by fitting a functional form any noise in the probability distribution is averaged over (the smoothing acts like a regularizing constraint). If a functional form were not used then the iterations could artificially amplify any noisy structures (this is a concern in using the iterative approach in image deconvolution, Richardson 1972; Lucy 1974, where such a simple functional form for the prior cannot be assumed). The 2D functional form in (e_1, e_2) we use is

$$\mathcal{P}(e_1, e_2) = A \cos\left(\frac{|e|\pi}{2}\right) \exp\left\{ -\left[\frac{2|e|}{B(1+|e|^D)}\right]^C \right\}, \tag{17}$$

where B, C and D are free parameters to be fitted and $|e| = \sqrt{e_1^2 + e_2^2}$. The prior is always normalized so that the parameter A is determined by the normalization. The cosine factor ensures that the prior goes to zero at $|e| = 1$. For $C \leq 1$ and $\neq 0$ the function has a cusp at $|e| = 0$, however the continuity of the function ensures symmetry about $|e| = 0$ which means that the derivative of the function is always zero at the origin.

We have found this function to be a good fit to both the STEP simulations' intrinsic distributions and the APM survey's published intrinsic ellipticity distribution (Crittenden et al. 2001). To convert to a 1D distribution in $|e|$ one must multiply by the appropriate parameter space volume factor, that is, $\mathcal{P}_{1D}(|e|) = 2\pi|e|\mathcal{P}(e_1, e_2)$. To fit the output prior from each iteration with this 2D functional form we minimize the *cross-entropy* defined as

$$H(p, q) = -\sum_x p(x) \log q(x), \tag{18}$$

where $q(x)$ is some estimated probability distribution and $p(x)$ is the 'true' distribution. This is similar to the Kullback–Leibler divergence between two distributions and is a measure of the difference between the two distributions $q(x)$ and $p(x)$. In our case we wish to minimize the difference between the functional prior and the output prior

$$H = -\sum_{e_1} \sum_{e_2} \mathcal{P}(e_1, e_2)_{\text{functional form}} \log \mathcal{P}(e_1, e_2)_{\text{output}}. \tag{19}$$

By minimizing this function the best-fitting functional form to the output prior is found. We found this to be more robust and yield better fits to the STEP intrinsic ellipticity distributions than projecting the distribution on to a 1D function of $|e|$ and using a binned least squares fitting method.

3.2 Testing the iterative approach with STEP

To test this iterative method we estimated the prior of the STEP1 simulations for PSF 0 from the zero-sheared image (PSF 0, image 0; see Section 4.1 for a full description of the STEP1 simulation) and compared the prior found with the input intrinsic ellipticity distributions used to create the simulated images. Fig. 2 shows the actual intrinsic ellipticity distribution in (e_1, e_2) for the STEP1 simulation and the prior found using the iterative approach. It can

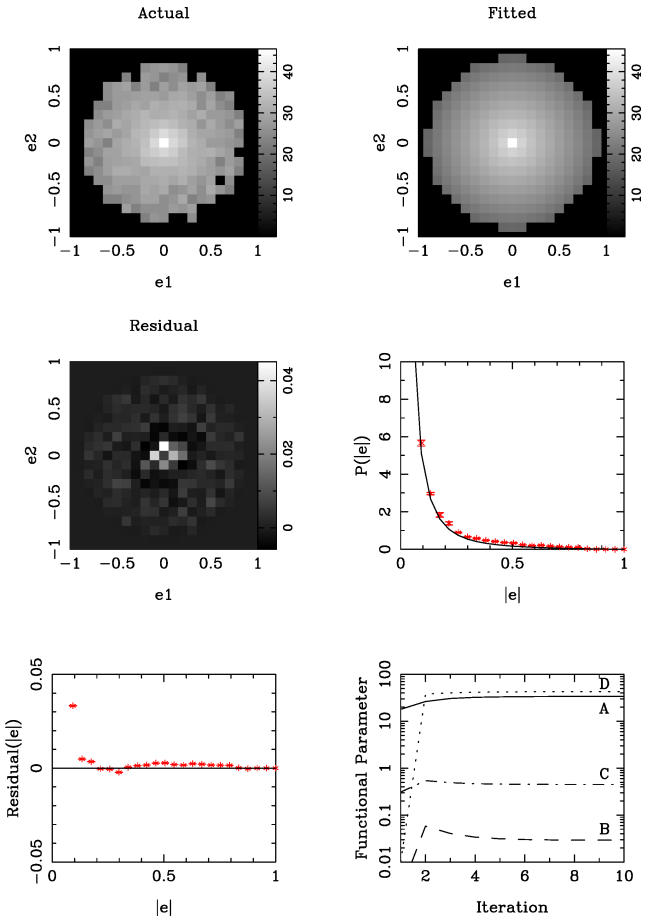

Figure 2. The top panels show the actual intrinsic ellipticity distribution used in the STEP1 simulations (top left-hand panel) and the prior created using the iterative method (top right-hand panel), where the distributions are normalised. The left-hand side of the middle panels shows the residual as a fraction of the actual distribution, i.e. $R = \Delta P/P = (P_{\rm true} - P_{\rm func})/P_{\rm true}$. The middle right-hand panel shows the azimuthally averaged 2D priors of the upper panels with the actual input prior (red points) and fitted prior (solid line). These include the the appropriate parameter space volume factor $P_{\rm 1D}(|e|) = 2\pi|e|P(e_1, e_2)$ and we have rescaled the y-axis for clarity. The lower left-hand panel shows the azimuthally averaged residual. The lower right-hand panel shows how the values of the parameters of the fitted functional form of the prior change as the number of iterations increases for parameter A (solid line), B (dashed line), C (dot–dashed line) and D (dotted line), see equation (17).

be seen from the very low level of fractional residual $\Delta P/P = (P_{\rm true} - P_{\rm func})/P_{\rm true}$ between the 'true' and the estimated prior, of order 0.02, that the iterative approach is an accurate and good method for finding the correct prior. Furthermore, the convergence to an accurate functional fit can occur in approximately five iterations. We tested the robustness of this convergence to the starting values of the functional parameters (A–D) and found that in all cases there was convergence in fewer than six iterations.

The correct prior is formally only a stable solution to the iterative approach in the case of an infinite ensemble of galaxies. Here, we present results that show the variation of the estimated prior as a function of the number of galaxies used in the iterative determination. There is no simple analytical way to determine the minimum number of galaxies required to determine the prior to a certain level of accuracy as this depends on the form of the prior. To accurately determine the prior probability surface the ellipticities of the galaxies used have to sample, to some degree, the whole (e_1, e_2) plane, that is, if a subset of galaxies were used that had exactly the same ellipticity they would not recreate the intrinsic distribution of the overall population using the iterative approach. In the limit of a small number of galaxies, from which the ellipticity is imperfectly determined, sample shot noise becomes an important factor. The accurate determination of the prior from a subset of galaxies from a population thus depends in a complex way on the shape of the likelihood surfaces and the number used. One may expect that $\sim$100 galaxies would not suffice since, with a resolution of $\Delta e = 0.1$, we evaluate the prior at $\lesssim$100 independent points in the (e_1, e_2) plane.

We numerically investigated the number of galaxies required to estimate the prior by selecting random samples of galaxies from the STEP1 PSF0 catalogue and recreating the prior using only these galaxies for many different random realizations of the subset. The prior created using these random subsets was then be compared to the prior found using the entire population. In Fig. 3, we show the best-fitting values of the functional parameters as the number of galaxies used to estimate the prior changes. For each galaxy subset number, we made 10 random samplings of the full catalogue, the lines show the mean values of the parameters averaged over these random samplings (after 10 iterations of the prior estimation algorithm). The errorbars show the variance in the values over the random samplings of the catalogue. This shows how the parameters fitted to the prior vary with the number of galaxies used to create the prior.

The value of the D parameter begins to deviate at a very low level when $\lesssim$500 galaxies are used. However, this parameter has a very small effect on the functional form. At $|e| \sim 0$ the D parameter only enters as a second order term in $|e|$ and so has a small effect. At $|e| \sim 1$ the cosine factor (in equation 17) dominates the functional form of the prior that suppresses any influence that the parameter D has on changing the behaviour of the function.

The deviation and variance in parameters B and C becomes significant when $\lesssim$100 galaxies are used, that is, the parameters that fit the prior depend strongly on the specific subset of galaxies, which are randomly chosen. This is demonstrated by the variance in the best-fitting values increasing in the top panel of Fig. 3 when fewer galaxies are used, and in addition the mean values deviate from the parameter values found using the whole population ($\sim$3000 galaxies) by a large amount. The bottom panel of Fig. 3 shows the rms value of the residual between the actual STEP1 input prior and the functional fit to the prior as a function of the number of galaxies used in the iterative approach. It is clear that the rms of the residual increases dramatically when the number of galaxies falls below $\sim$300.

When analysing the STEP simulations, in which there are a small number of galaxies per image, the problem of too few galaxies with which to recover the prior will be encountered. This is discussed in Section 4.2 where we find that in the STEP2 simulations the intrinsic ellipticity varies as a function of size and magnitude, and that by correctly accounting for this variation the shear estimation does improve. In an actual survey in which the number of galaxies is $\gg 10^4$ one would expect that in any subpopulation of galaxies, defined by some commonly observed property such as magnitude, size, colour or type, there would be $\gg$100 galaxies, so that this problem will not arise when the method is used on large data sets.

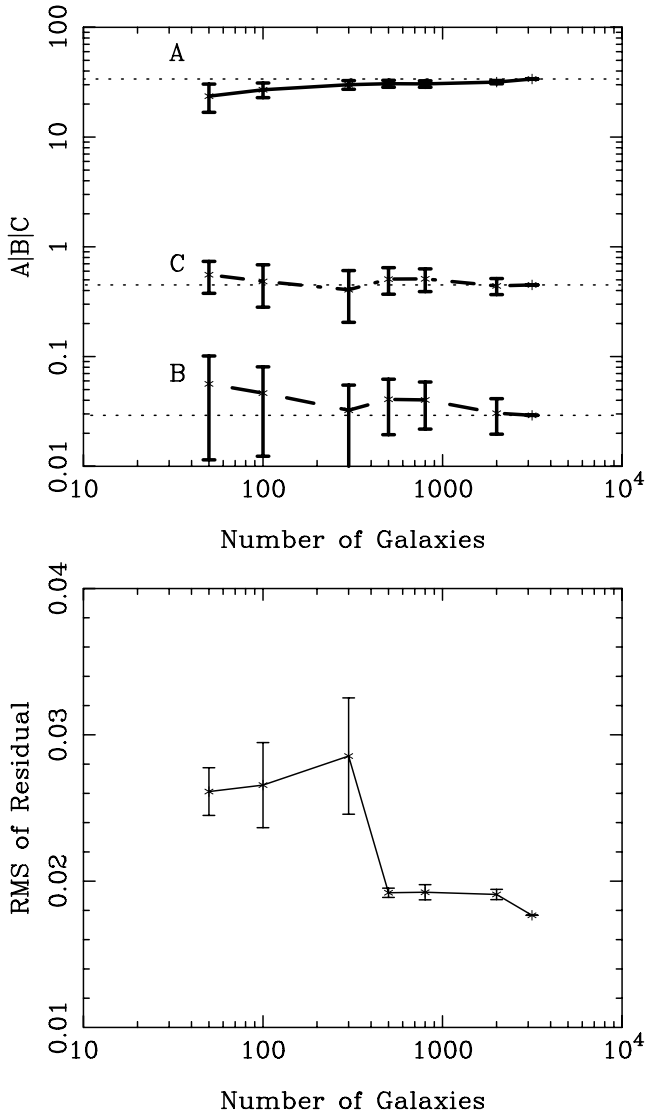

Figure 3. The top panel shows the variation in the parameter values, from equation (17), found by recovering the prior using the iterative approach (after 10 iterations) as a function of the number of galaxies used in the prior estimation. For each galaxy number bin we selected ten random subpopulations of the entire sample of galaxies. The bold black lines show the mean and the variance of the parameter values over all the random samplings. We show parameters A = solid line, B = dashed line, C = dot–dashed line, the dotted horizontal lines show the values of these parameters when the whole galaxy sample is used. We do not show the variation of D for clarity, and since the value of D has a small effect on the functional form of the probability; the value of D begins to deviate below ∼500 galaxies. The bottom panel shows how the rms of the fractional residual between the actual STEP1 input prior and the functional fit to the prior, i.e. $R = \Delta P/P = (P_{\rm true} - P_{\rm func})/P_{\rm true}$, varies with the number of galaxies used to create the prior. The mean is the average rms over all random samplings of the full input catalogue, the error on each point shows the variance of the rms over the random samplings.

3.3 Summary of the lensfit shape measurement method

Before presenting the results of using LENSFIT on simulations, we summarize the method. We consider the $i = \{1, 2\}$ shear component g_i, where $\boldsymbol{g} = g_1 + ig_2$ and $\boldsymbol{e} = e_1 + ie_2$. We also recast any integrals as summations, as is done in the actual LENSFIT implementation.

(i) We use a Bayesian estimator of shear that is given by the summation over N galaxies:

$$\hat{g}_i = \frac{\sum_\alpha^N \langle e_i \rangle_\alpha}{\sum_\alpha^N |\partial \langle e_i \rangle_\alpha / \partial g_i|}, \tag{20}$$

where $\partial \langle \boldsymbol{e} \rangle_\alpha / \partial \boldsymbol{g}$ is the *shear sensitivity* (Miller et al. 2007) and we sum over galaxies α.

(ii) The expectation value of the ith ellipticity value for an individual galaxy α is given by

$$\langle e_i \rangle_\alpha = \int {\rm d}e_j \int {\rm d}e_i e_i \, p_\alpha(e_i, e_j) \approx \sum_j \sum_i \Delta e^2 e_i \, p_\alpha(e_i, e_j), \tag{21}$$

where $p_\alpha(e_i, e_j) = \mathcal{P}(e_i, e_j)\mathcal{L}_\alpha(e_i, e_j)$ is the posterior ellipticity probability distribution for a given galaxy.

(iii) To calculate the likelihood as a function of ellipticity we use a model fitting approach that marginalizes over position and amplitude in an analytic way and fits a exponential profile. Using equation (13) the likelihood is then given as a function of radius r and ellipticity e_1 and e_2. This is then analytically marginalized over radius using

$$\mathcal{L}(e_1, e_2) \approx \sum_{r_{\rm min}}^{r_{\rm max}} \mathcal{L}(e_1, e_2, r) \Delta r, \tag{22}$$

where we assume a uniform prior in r.

(iv) The shear sensitivity is recast from equation (8) as

$$\frac{\partial \langle e_i \rangle_\alpha}{\partial g_i} \simeq 1 - \frac{\sum_j \sum_i \Delta e^2 \left(\langle e_i \rangle - e_i \right) \mathcal{L}_\alpha(e_i, e_j) \dfrac{\partial \mathcal{P}(e_i, e_j)}{\partial e_i}}{\sum_j \sum_i \Delta e^2 \mathcal{P}(e_i, e_j) \mathcal{L}_\alpha(e_i, e_j)}. \tag{23}$$

(v) The prior $\mathcal{P}(e_i, e_j)$ is a zero-centred function that is representative of the intrinsic ellipticity distribution. We calculate this using a stable iterative approach in which the data itself can be used to estimate the prior.

4 RESULTS OF TESTS ON SIMULATIONS

In the following section we describe the simulations in detail, and present the results of recovering the input shear from these simulations using LENSFIT, we also compare with the currently published STEP1 and STEP2 results.

The ability of a shape measurement method to recover the input shear from a simulation in the STEP papers is parametrized by

$$\gamma_i^M - \gamma_i^T = m_i \gamma_i^T + c_i, \tag{24}$$

where γ_i^T is the 'true' (input) shear for the ith shear component and γ_i^M is the 'measured' or estimated shear value using a given shape measurement method. m_i characterizes any bias in a shape measurement method, c_i characterizes any residual shear offset. Any residual shear offset is usually due to inaccuracies in the PSF estimation, as a PSF that is slightly more elliptical than reality will simply act to add a constant to any estimated shear value. In STEP1, some methods also require a quadratic term on the *LHS* side of equation (24), $q(\gamma_i^T)^2$. We have found that the LENSFIT results do not require the quadractic term hence we will present the results in terms of m_i and c_i in line with the STEP papers.

4.1 Application to the STEP1 simulations

STEP1 (Heymans et al. 2006) created simulated galaxies that consist of a de Vaucouleurs bulge plus an exponential disc. The simulations are provided with six different PSFs (named 0–5), and for each PSF

there are five shear sets each consisting of an ensemble of 64 individual images of 4096 pixels × 4096 pixels. The five shear sets for each PSF have different shear values of $\gamma_1 = 0.0, 0.005, 0.01, 0.05$ and 0.10; $\gamma_2 = 0.0$ is set for all the STEP1 simulations. Each of the shear sets (64 images) contains $\sim 2 \times 10^5$ galaxies. Each image also contains ∼3000 stars from which the PSF can be determined, the pixel scale in the simulations is 0.206 arcsec and the average PSF full width at half-maximum is 0.8–0.9 arcsec.

In order to test the LENSFIT method we used SEXTRACTOR (Bertin & Arnouts 1996) to create input catalogues from the STEP1 simulations to find the positions of the galaxies and stars. For each image in each PSF set and for each shear value we recalculated the PSF from the stars available in that image. We calculated the prior, as described in Section 3, using the zero-shear image from each PSF set.

For the error on the shear estimate γ_i and hence $\gamma_i^M - \gamma_i^T$ for each image we use the error on the mean ellipticity given for N galaxies by $\sigma_M = \sigma/\sqrt{N}$. The expectation value $\sigma^2 = \langle e_i^2 \rangle / (\partial \langle e \rangle_i / \partial g_i)$ is calculated by integrating over the posterior probability as in equation (21). We then use a χ^2 fit to $\gamma^M - \gamma^T$ as a function of γ^T to find the best-fitting values of m_i and c_i defined in equation (24). The errors on m_i and c_i are found by exploring the whole (m_i, c_i) parameter space and projecting the two parameter 1σ errors on to the corresponding axis to find the 1σ error on each parameter.

Fig. 4 shows the measured shear minus the true (input) shear $\gamma^M - \gamma^T$ for PSF 0 of the STEP1 simulations with the best-fitting linear function from equation (24).

Fig. 5 shows the results of applying the LENSFIT method to the STEP1 simulation. For STEP1 we find m_1 and c_1 (bias and offset of the measured γ_1 values), we also find c_2 assuming that $m_2 = 0$, as in the STEP1 publication. $\langle m \rangle$ is the average bias over all PSFs, and the error on this value is the sum of the squares of the errors on m from each PSF. σ_c is the average variance in the offset from c_1 and c_2, i.e. $\sigma_c = \sqrt{\sigma_{c1}^2 + \sigma_{c2}^2}$. The result is detailed in Table 1.

The value of $\langle m \rangle = +0.006 \pm 0.005$ is the smallest for any method for which a linear fit to $\gamma_i^M - \gamma_i^T$ is required (Heymans et al. 2006). The methods that require a non-linear term in equation (24), q, are shown by a circle about the point in Fig. 5. $q > 1.3$ for all these methods and, as shown in fig. 2 of Heymans et al. (2006), this parametrizes large non-linear effects. In our results there is no motivation for a non-linear term. We find minimum $\chi^2 \sim 1.7$ with 3 degrees of freedom, therefore we find no extra parameters are warranted. The value of $\sigma_c = 0.0002$ is smaller than any method in the STEP1 publication. This value parametrizes any PSF systematics: in the absence of systematics and shot noise for a perfect shape measurement method one would expect $\sigma_c = 0$.

We also present a preliminary analysis of the dependence of the bias and offset on galaxy type. The success of the method on the bulge plus disc galaxies in the STEP1 simulations (and using the STEP2 shapelet galaxies – see Section 4.2) suggests that the method is robust to the type of simulated galaxy. One may expect that the assumption of a particular model may bias the model-fitting class of shape measurement method, where a model is implicitly assumed, however in the low signal-to-noise ratio limit all profiles can be approximated by a simple exponential form. In Fig. 6, we show the bias and offset in γ_1 using PSF0 using three different galaxy selection criteria. The criteria are somewhat arbitrary since in the STEP1 simulations there is a continuous range of galaxies containing different proportions of (exponential) disc and (de Vaucouleurs) bulge. It can be seen that LENSFIT has a bias of $|m| < 0.02$ for all simulated galaxy types in STEP1. The errorbars are a reflection of the number of galaxies in each type bin, for the dominantly

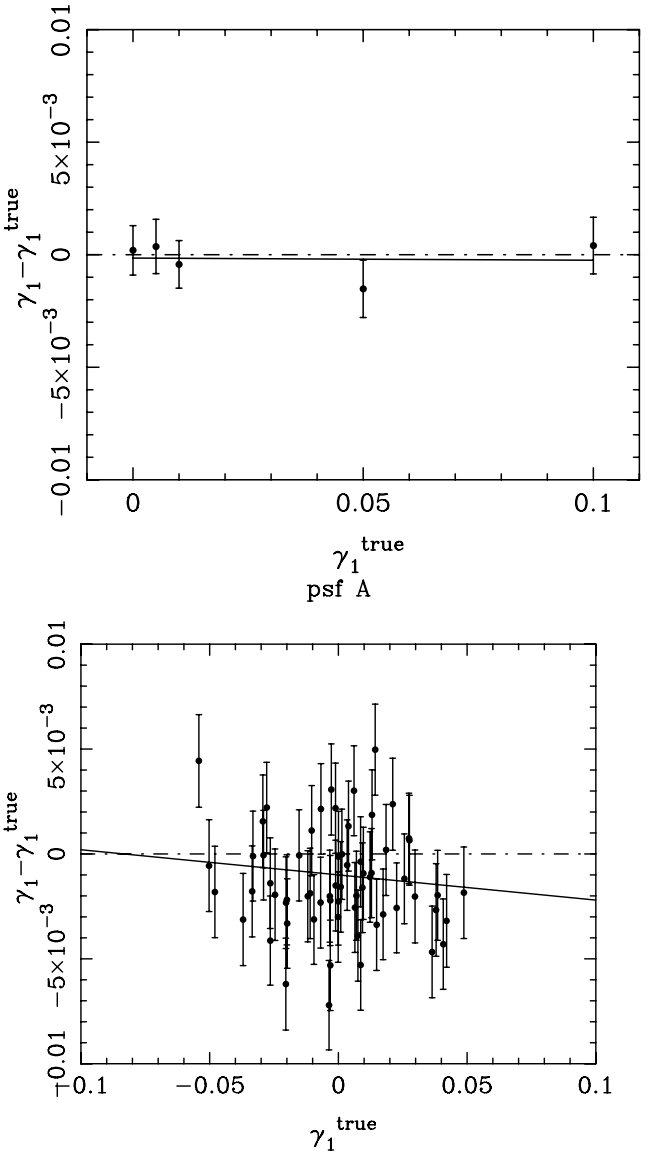

Figure 4. The upper panel shows the estimated γ_1 shear values minus the true (input) $\gamma_1^{\rm true}$ shear for STEP1 PSF 0, for STEP1 only five input shear values are provided. The upper solid line shows the m_1 and c_1 fit for STEP1 PSF 0 ($m_1 = -0.0009$, $c_1 = -0.0002$). The lower panel shows the estimated γ_1 shear values minus the true (input) $\gamma_1^{\rm true}$ shear for STEP2 PSF A simulations, the solid line shows the best linear functional fit $m_1 = -0.012$ and $c_1 = -0.000\,99$. There are 64 images, with random shear values distributed within the range $-0.06 \leq \gamma_1 \leq 0.06$, that are used to estimate the shear for each point in the upper panel whereas only two images per point are used in the lower panel.

exponential and de Vaucouleurs sets the number of galaxies in each image catalogoue are $\lesssim$200 and $\lesssim$500, respectively hence the deviation away from $m \equiv 0$ and $c \equiv 0$ for the exponential population is purely statistical. The fitting does not improve when galaxies are chosen which have the same profile as the underlying model (an exponential), this shows that the method is not biased by the assumed model, and confirms the expectation that in the low signal-to-noise ratio limit the majority of galaxy profiles can be approximated by an exponential.

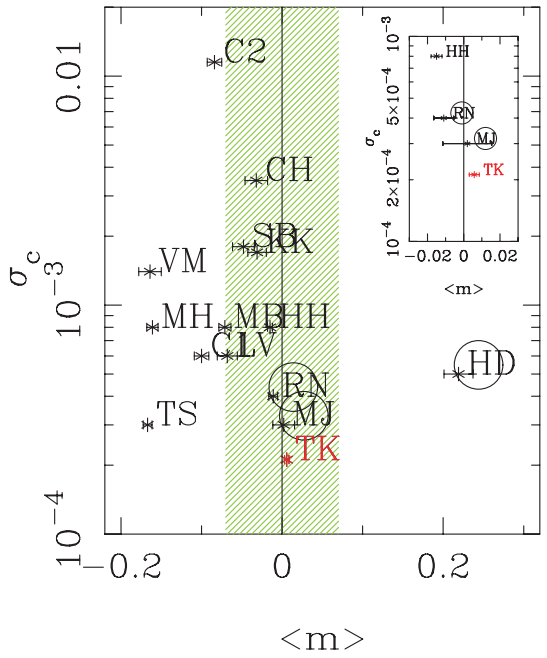

Figure 5. Adapted from Heymans et al. (2006), Fig. 3. The average value of the bias m over all PSFs in the STEP1 simulation and the variation in the offset σ_c. The red point 'TK' shows the result of using LENSFIT, the black points show the other shape measurement methods presented in Heymans et al. (2006) (the labelling reflects the authorship of the method, see table 2 of Heymans et al. 2006 for more details). The points surrounded by circles are those that required an extra quadratic term in equation (24). The hatched region indicates the level of precision required by current surveys ($\langle m\rangle \leq 0.07$), as discussed in Heymans et al. (2006). The inset shows a zoom in of the bottom part of the figure.

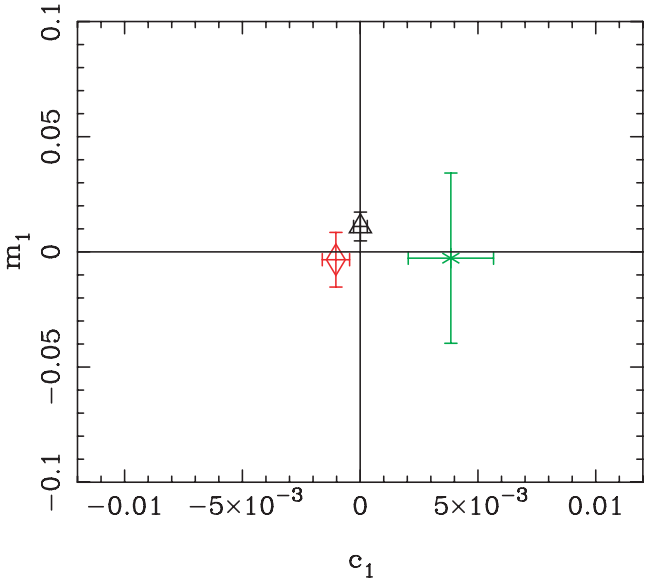

Figure 6. Type dependence of the bias m_1 and offset c_1 in the measured shear using the STEP1 simulation and PSF0. The type selection has been done using B the 'bulge to total flux ratio' provided in the STEP1 simulations. The points are labelled as: red ($\diamond$) dominantly de Vaucouleurs $B \leq 0.3$, black ($\triangle$) mixed profiles $0.3 < B \leq 0.7$ and green ($\times$) dominantly exponential $B > 0.7$.

4.2 Application to the STEP2 simulations

This section presents the results of extracting shear estimates using LENSFIT from the STEP2 (Massey et al. 2007b) simulations. These simulations consist of shapelet based (Refregier 2003; Massey et al. 2004; Massey & Refregier 2005) and exponential galaxy profiles convolved with various PSFs. There are six sets of PSF and galaxy profile combinations provided. Sets A, C, D, E and F have shapelet simulated galaxies and various PSF shapes. Sets D and E have highly elliptical PSFs aligned along the e_1 and e_2 directions, respectively. Set B has the same PSF shape as A but with exponential galaxies as opposed to shapelet galaxies. Each set consists of 64 images and 64 'rotated' images. The rotated simulated galaxies are the

Table 1. The STEP1 and STEP2 m and c results.

Data set	Galaxy sample	$\langle m\rangle$	$\sigma(\langle m\rangle)$	$\langle c\rangle$	$\sigma(\langle c\rangle)$	N
STEP1						
All PSFs	SExtractor catalogue	+0.0058	0.0056	−0.0006	0.0002	9
STEP2						
All PSFs	SExtractor matched catalogue	+0.0020	0.0163	−0.00071	0.00063	30
No PSF D & E	SExtractor matched catalogue	+0.0010	0.0159	−0.00025	0.00063	29
All PSFs	$18 \leq \mathcal{M} < 20$	−0.0640	0.1294	−0.0029	0.0032	0.2
All PSFs	$20 \leq \mathcal{M} < 21$	−0.0167	0.1235	+0.0020	0.0030	0.8
All PSFs	$21 \leq \mathcal{M} < 22$	+0.0134	0.0258	+0.0015	0.0006	2
All PSFs	$22 \leq \mathcal{M} < 23$	+0.0019	0.0251	−0.0011	0.0006	6
All PSFs	$23 \leq \mathcal{M} < 24$	−0.0177	0.0281	−0.0003	0.0007	13
All PSFs	$24 \leq \mathcal{M} < 25$	−0.0049	0.0662	−0.0033	0.0016	7
All PSFs	$0.2 \leq \mathcal{R} < 0.4$	+0.0027	0.0152	−0.0028	0.0011	15
All PSFs	$0.4 \leq \mathcal{R} < 0.6$	+0.0094	0.0113	−0.0015	0.0003	7
All PSFs	$0.6 \leq \mathcal{R} < 0.8$	+0.0031	0.0260	+0.0001	0.0007	2
All PSFs	$0.8 \leq \mathcal{R} < 1.0$	−0.0192	0.0370	−0.0005	0.0009	0.7
All PSFs	$1.0 \leq \mathcal{R} < 1.2$	−0.0130	0.0559	−0.0041	0.0013	0.2

Note. We use galaxies in the catalogues created using SExtractor, for STEP2 we match the rotated and unrotated catalogues. N is the average number density of galaxies per square arcminute, for STEP2 this is the number in the matched catalogues. For STEP2 PSF A contains a slightly higher than average matched number density 32 per square arcminute, and PSF C contains slightly lower than average 26 per square arcminute. The lower two sections show how the STEP2 results vary with magnitude $\mathcal{M}$ and size/radius $\mathcal{R}$, the magnitude is the SExtractor magnitude calibrated using the STEP2 zero-point of $\mathcal{M}_0 = 30.8$ and the radii are assigned using a shapelet based definition described in Massey et al. (2007b).

same as the 'original' images except that they have been rotated by 90° before being sheared. As described in Massey et al. (2007) this allows the intrinsic shape noise to be dramatically reduced by co-adding the shear estimates from the matching corresponding images. The signal-to-noise ratio error on the intrinsic ellipticity is usually given for a sample of N galaxies as (equation 3, Massey et al. 2007)

$$\sigma(\langle e^{\rm int}\rangle) = \sqrt{\frac{\langle (e_i^{\rm int})^2\rangle}{N}}. \quad (25)$$

Massey et al. (2007b) showed that by defining the average shear as the average of the observed ellipticities from the rotated and unrotated galaxy images, $\tilde{\gamma} = (e^{\rm obs,unrot} + e^{\rm obs,rot})/2$, the shot noise error on the average shear is reduced to (equation 6, Massey et al. 2007)

$$\sigma(\langle e^{\rm int}\rangle) = \sqrt{\frac{\langle (e_i^{\rm int})^4\rangle}{2N}}. \quad (26)$$

In STEP2, the averaging is done on a galaxy-by-galaxy basis, that is, each galaxy paired with its rotated counterpart. We calculate the shear by taking the mean expected ellipticity weighted by the shear sensitivity $\tilde{\gamma} = (\langle e^{\rm obs,unrot}\rangle + \langle e^{\rm obs,rot}\rangle)/2$, giving equal weight to the unrotated and rotated probability surfaces.

Each image (and corresponding rotated image) contains ∼1500 galaxies that are usable for shear (the images actually contain ∼5000 galaxies but the majority are too faint to be detected), and has a different random shear, γ_1 and γ_2, applied. The shear values are randomly chosen in the range $\gamma \leq 0.06$. For each set (PSF) a star field is provided that contains ∼240 stars (and no galaxies) which can be used to estimate the PSF, the galaxy fields also contain stars that can be used instead of, or in addition to, the stars provided in the star fields. The simulations are a sophistication of the STEP1 simulations in two important ways. First the galaxies are 'more realistic', that is they are mostly shapelet galaxies some of which exhibit substructure, spiral arms etc. This should be a significant test for LENSFIT which assumes exponential profiles. Secondly the shear values are varied randomly in both the γ_1 and γ_2 directions as opposed to sampling just five points in γ_1 and setting γ_2 to be zero as is the case in STEP1. In this case there will be m_i and c_i values associated with γ_1 and γ_2; m_1, m_2, c_1, c_2.

To implement the LENSFIT method we used SExtractor (Bertin & Arnouts 1996), on each set of PSF images to create a catalogue for the rotated and unrotated sets of images, we then created a matched catalogue in which we kept only galaxies that were detected in both rotated and unrotated catalogues. For each PSF the positions of the galaxies are the same over every image (shear value). We measured the PSF from the starfield images by using SExtractor to identify the star positions. For PSFs D and E we also used the stars that were detected in the galaxy images and co-added this to the PSF from the starfield since a poor characterization of these highly elliptical PSFs could affect the shear found from these sets of images as seen in Massey et al. (2007).

For the global shear estimates we used every galaxy in the matched catalogues to determine the intrinsic ellipticity prior from the zero-shear image provided for each PSF, that is, the prior was averaged over all size and magnitude ranges. For the investigation into the size and magnitude dependence of the estimated shear using these simulations we recreated the prior for each size and magnitude bin using only the galaxies in that bin. We found that the prior exhibited significant variation over the magnitude and size ranges investigated.

We calculate the errors on $\gamma_i^M - \gamma_i^T$ and hence the best-fitting values of m_i and c_i with associated errors in the same way as for STEP1, described in Section 4.1. This results in a most likely value for m_i and c_i for each PSF with associated errors, Fig. 4 shows the linear fit to $\gamma_i^M - \gamma_i^T$ for the PSF A set of shear values. The average $\langle m\rangle$ and $\langle c\rangle$ is taken over all the values from each PSF and over γ_1 and γ_2. The error presented on the average is the same as presented in Massey et al. (2007) which is the *average of the errors* over all PSFs

$$\bar{\sigma}(\langle m\rangle) = \frac{\sum_{\rm psf}\sigma(m_{\rm psf})}{N_{\rm psf}}, \quad (27)$$

where $N_{\rm psf}$ is the number of PSFs. This is meant to produce an error that is indicative of the expected error that one should get when using a particular shape measurement method on a data set.

Bias and offset for the whole STEP2 catalogue

For the analysis of the entire catalogue we make no additional size or magnitude cuts other than those implicit in the SExtractor source extraction, we use every galaxy in the matched catalogue for each image in each PSF set. Fig. 7 shows the best-fitting m_i and c_i values for γ_1 and γ_2 for each PSF. It can be seen that there is no general pattern or offset in the values: the individual values of the biases and offsets for any individual PSF are consistent with that expected if the points were randomly scattered about ($m = 0$, $c = 0$) with a dispersion due to the finite size of the galaxy sample. The value of c_1 is slightly systematically offset from $c_1 = 0$, we discuss this later in this section. Fig. 8 shows that the scatter in bias is indeed statistical since when averaging over all PSFs the value of $\langle m\rangle \sim 0.002 \pm 0.016$. The results are presented in detail in Table 1. This shows that the LENSFIT method has a smaller bias than any method presented in the STEP2 publication (Massey et al. 2007). Furthermore, the most likely values of m and c do not vary substantially when PSF D and E, that have the strongest PSF distortions, are removed. This suggests that the scatter in Fig. 7 is indeed purely statistical. The errorbars do not increase since they are the average errors on m and c for the PSFs used, see equation (27). We find minimum $\chi^2 \sim 60$ for the linear fit to the STEP2 results (compared to 62 degrees of freedom), as such we find no extra parameters, for example an extra quadratic term in the $\gamma^M - \gamma^T$ functional fit, are warranted.

The errors on m and c in Fig. 8 are larger than some of the methods in STEP2 and similar to other methods' errors. We do not have enough information to comment on the relative size of the errorbars between the different methods in this paper. However, in Section 5 we do investigate the measured shear variance of the LENSFIT method and show that it is close to the expected variance from the simulations, this is shown in Fig. 11. In practice one could design an additional weighting scheme to supplement equation (7) (as in Miller et al. 2007; equation 3) in order to improve the shear estimation even further, we leave this optimization for future work.

The slightly larger value of $\langle c\rangle$ relative to the other STEP2 methods is possibly due to residuals in the PSF estimation. We make this assertion since a systematic error on PSF estimation is the most straightforward way to create a non-zero c value and also because we have identified pixelization of the PSF as a potential source of limitation. Whilst the value of c is larger we do note a number of points that are relevant to this issue. First it has been shown (for example in Kitching et al. 2008a) that it is the bias m not an offset c in the estimated shear that has the largest effect on cosmological parameter estimation. Furthermore, planned space-based wide field imagers such as DUNE and SNAP will have very stable PSF

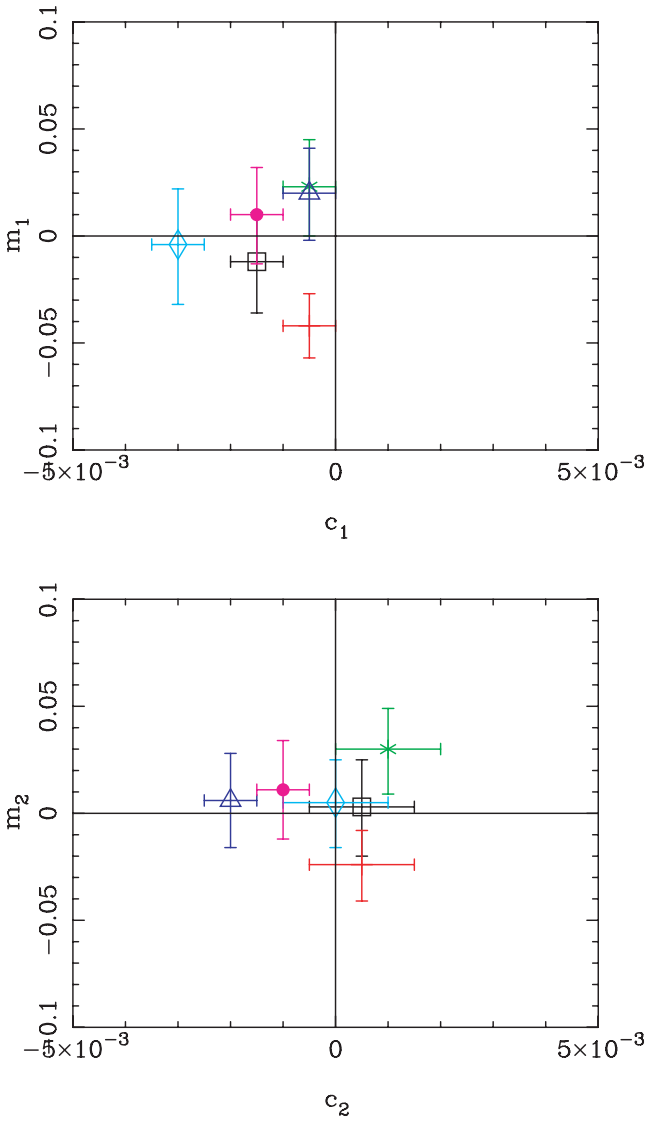

Figure 7. The top panel shows the best-fitting m_1 and c_1 values with errors for the STEP2 simulations. The bottom panel shows the best-fitting m_2 and and c_2 values. In both panels black (□) =PSF A, red (+)=PSF B, green (×)= PSF C, blue (△)= PSF D, cyan (◇) = PSF E, magenta (•)= PSF F.

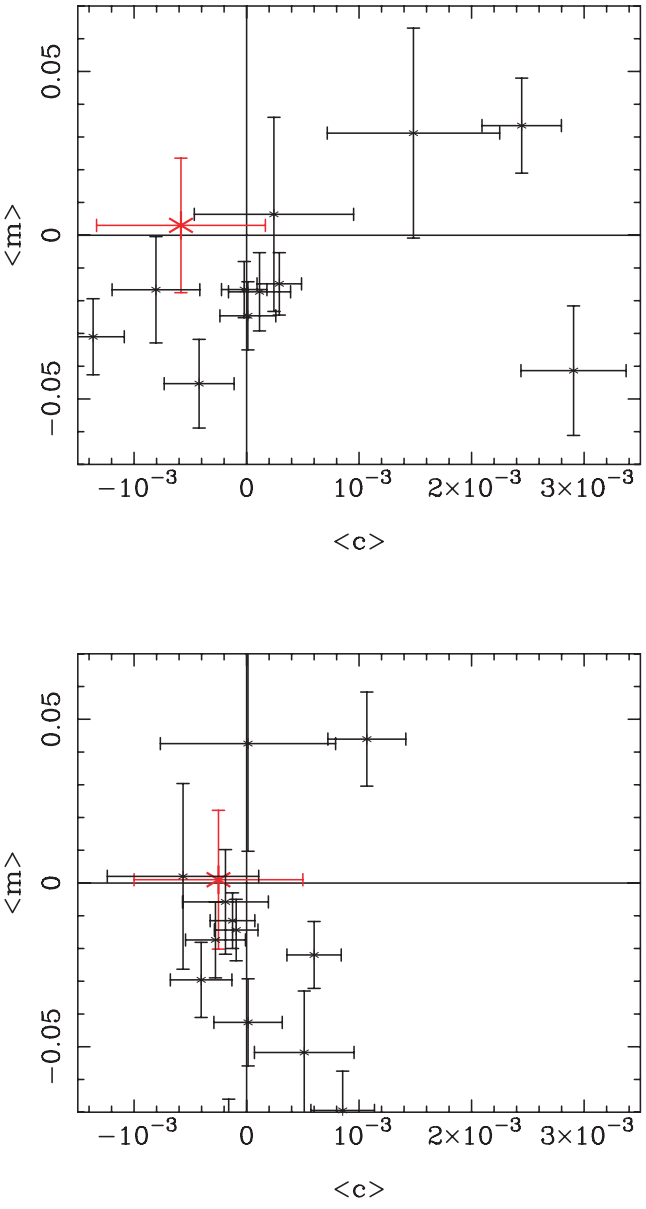

Figure 8. Adapted from Massey et al. (2007b), Fig. 6. The red points (in larger font) show the result of using LENSFIT on the STEP2 simulations. The black points show other shape measurement methods analysed in Massey et al. (2007b). The top panel shows the value of m and c, averaged over all PSFs and γ_1 and γ_2. The bottom panel shows the value of m and c averaged over PSFs A, B, C and F, that is, with the highly elliptical PSFs D and E ignored. The errors shown are the average of the errors on each PSF, equation (27).

modelling at high resolution before launch. We also note that the way in which the PSF is determined is not central to the method, for example any PSF determination routine could be used (e.g. polynomial or shapelet reconstruction) in conjunction with the unbiased shear estimation method to reduce the c value.

Bias and offset as a function of size and magnitude

Here we show how the bias and offset vary as a function of magnitude $\mathcal{M}$ and size/radius $\mathcal{R}$, the detailed results are summarized in Table 1. The SExtractor matched catalogues used were set to the zero-point of $\mathcal{M}_0 = 30.8$ as discussed by Massey et al. (2007). The value of the size of the galaxy used a shapelet based definition (Massey & Refregier 2005; equation 53) and these values were obtained for each galaxy we detected from the STEP2 website.[5]

[5] http://www.physics.ubc.ca/~heymans/step/step2_info.html

Positions were not obtained from the website. We re-iterate that the intrinsic ellipticity prior was recalculated for each magnitude and size bin, always assuming a zero-sheared functional form as described in Section 3. The extent of the magnitude and size ranges used here differs slightly from that used in the STEP2 publication since we find on average less than 2 galaxies in the magnitude range $\mathcal{M} = 25$–26 or the size range $\mathcal{R} = 1.2$ to 1.4 arcsec. For each magnitude bin the whole range of galaxy sizes is used, and for each size bin the whole magnitude range is used (though of course maginitude and size are highly correlated quantities).

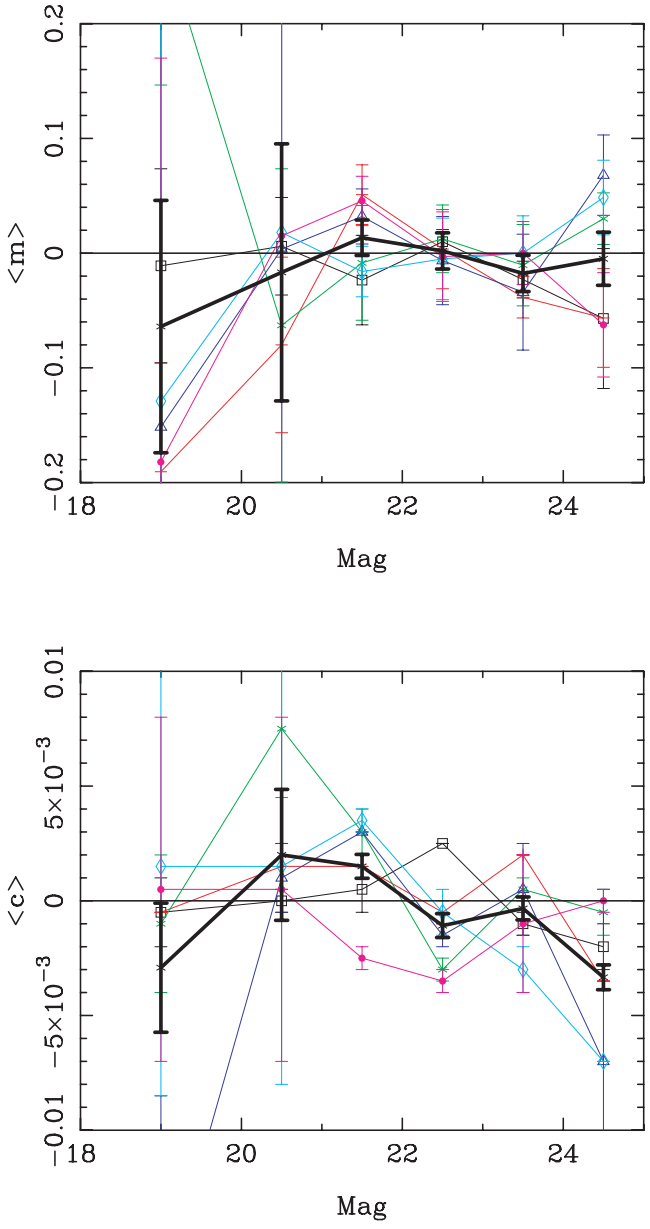

Figure 9. The variation in the bias $\langle m \rangle$ and offset $\langle c \rangle$ as a function of magnitude for the STEP2 analysis. The fainter coloured lines are the values from each individual PSF; in both panels for the fainter lines black (□) =PSF A, red (+)=PSF B, green (×)=PSF C, blue (△)=PSF D, cyan (◇) =PSF E, magenta (•)=PSF F. The bold black lines show the average over all PSFs. The points in magnitude are at the centre of the bin used, see Table 1 for the values of the bin boundaries used. The errors on the average over all PSFs are the average of the errors from each individual PSF, as discussed in Section 4.2. The average errorbars do not represent the scatter in the mean values of the individual PSF points.

Fig. 9 shows how the bias m and offset c vary as a function of the magnitude of the galaxies. The fainter coloured lines show how this varies for each individual PSF, averaged over γ_1 and γ_2, the bold black lines show the average $\langle m \rangle$ and $\langle c \rangle$ over all PSFs. There is a scatter of values from each PSF about the $\langle m \rangle = 0$ line, however this is dominantly statistical since, when taking the average, the bias is $|\langle m \rangle| < 0.02$ for $20 < \mathcal{M} < 24$. The deviation at $\mathcal{M} < 20$ is due to the number of galaxies in this bin being small (<10), however the errorbars show that the points' variation from $\langle m \rangle = 0$ is not statistically significant. The weak variation of $\langle c \rangle$ as a function of magnitude shows that the method is robust to the magnitude range used. The only deviations from $\langle c \rangle = 0$ occur where the number of galaxies in the bin becomes very low at $\mathcal{M} < 20$ and at the faintest magnitudes $\mathcal{M} > 24$. The method performs better in certain magnitude bins than when the sample is taken as a whole because the intrinsic ellipticity prior, which is recalculated for each magnitude bin, now better represents the intrinsic distribution of ellipticities in that bin. The variation of the intrinsic ellipticity distribution was an issue highlighted in the STEP2 publication (Massey et al. 2007). By taking a global average this information is averaged over, so that the global prior is less representative of some galaxy subpopulations. This highlights the need to calculate the prior as a function of galaxy properties; in STEP2 we only investigated magnitude and size dependence but this could be extended to colour or galaxy type.

Fig. 10 shows the variation in $\langle m \rangle$ and $\langle c \rangle$ as function of galaxy size, and as in Fig. 9 the fainter lines show the values for each PSF individually and the bold line shows the average over all PSFs. The variation in the bias over the whole range in size is $|\langle m \rangle| \lesssim 0.02$ with no point being a statistically significant deviation from $\langle m \rangle = 0$. The variation of the offset as a function of size is very small in the range $0.6 < \mathcal{R} < 1.0$ arcsec. Again, the method performs better in certain size bins than when the galaxy sample is taken as a whole.

The deviation at $\mathcal{R} > 1.0$ arcsec is again due to the very small average number of galaxies (<10) in this bin, however even with this small number of galaxies the bias is unaffected. There is also a deviation in the offset at $\mathcal{R} < 0.6$ arcsec, however the STEP2 pixel scale is 0.2 arcsec pixel^{-1} so that galaxies in the bin $0.2 < \mathcal{R} < 0.4$ arcsec have scales of only ∼1–2 pixels.

4.3 Discussion

In Section 4.1, we presented the results of using the LENSFIT method on the STEP1 and STEP2 simulations. The performance of the method was parametrized by calculating the difference between the input shear value for a given image and the estimated shear from that image. This quantity was then fitted, as a function of input shear, with a linear function. The function is parametrized by a bias m and an offset c, defined in equation (24). The results of this application to the simulations were summarized in detail in Table 1.

We found that the method performed very well in comparison to the other methods presented in the STEP publications. In particular the bias m is smaller in both the STEP1 and STEP2 simulation results than the majority of methods, and performs consistently well over the whole suite of simulations. The small residual bias in the STEP1 simulation might be attributed to inaccuracies in the PSF characterization due to pixelization effects, see Section 2.4. In STEP2 we found again that the bias m was small in comparison to other methods. Furthermore when two of the PSFs were removed, the most elliptical PSFs (D and E) the best-fitting values of the m and c values change by a very small margin, this suggested that the scatter in the values, shown in Fig. 7 is entirely statistical and due to the finite, number of galaxies in each STEP2 image.

Of course, there is the caveat that there could exist galaxies that have morphological types that are not included in the simulations. However we have found that the LENSFIT method performs well over all simulated morphological types upon which it has been tested (exponential, de Vaucouleurs, shapelet). In addition, one may be concerned that the source extraction routine used may bias the results by preferentially selecting a galaxies with particular properties.

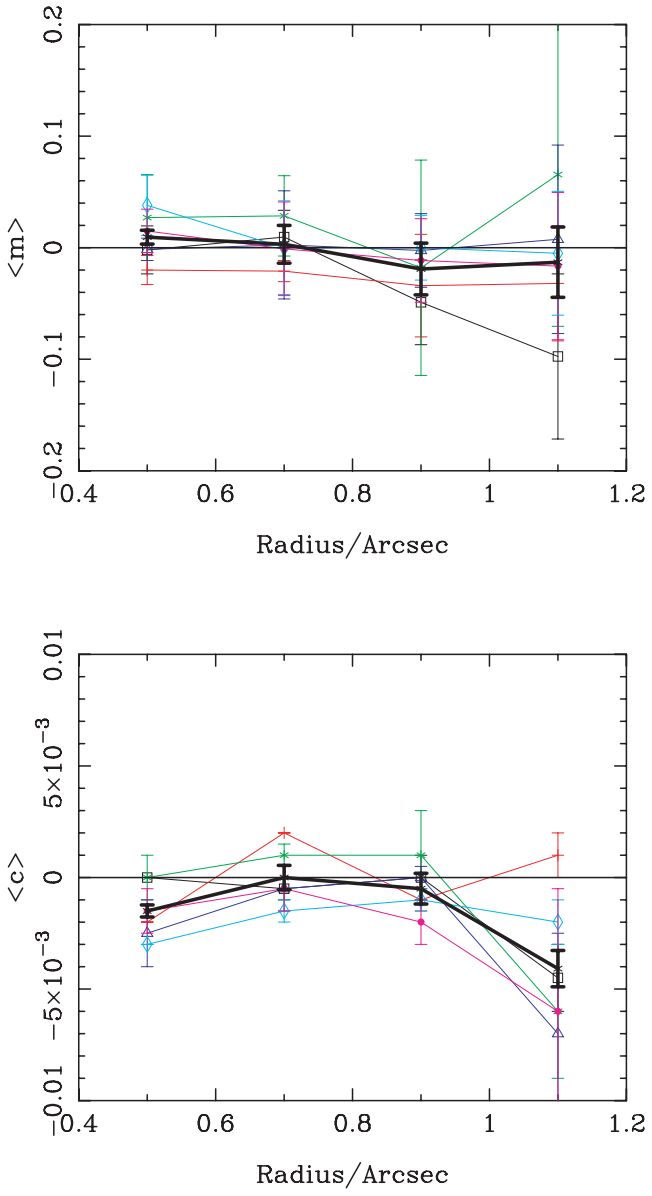

Figure 10. The variation in the bias $\langle m \rangle$ and offset $\langle c \rangle$ as a function of size for the STEP2 analysis. The size of a galaxy is defined as its radius, and is shown in units of arcseconds, where the pixel scale of the STEP2 simulations is 0.2 arcsec pixel^{-1}. The fainter coloured lines are the values from each individual PSF; as in Fig. 9. The bold black lines show the average over all PSFs. The points in radius are at the centre of the bin used, see Table 1 for the values of the bin boundaries used. The errors on the average over all PSFs are the average of the errors from each individual PSF, as discussed in Section 4.2. The average errorbars do not represent the scatter in the mean values of the individual PSF points.

However since we have used a realistic source extraction routine and found similar number densities to those used by other shape measurement methods in the STEP publications we not expect selection effects to significantly bias the method in real data.

We now refer to table 1 in Massey et al. (2007b). To summarize, all STEP2 PSFs use shapelet galaxies except PSF B which uses exponential profiles, PSF A and B are the same SUBARU PSF but use different galaxy types. PSF C is an enlarged PSF, and PSFs D and E are highly elliptical aligned along the x (e_1) and 45° (e_2) axes, respectively. PSF F is circularly symmetric. It can be seen from Fig. 7 that there is no pattern in the best-fitting values of the bias m and offset c as function of galaxy type or PSF. The PSF for which these values is largest is C. This could be due to the slightly lower number density of matched galaxies for PSF C, 26 per square arcmin (which is consistent with other methods in Massey et al. 2007 all of which find a lower number density for PSF C). There is no statistically significant difference between the exponential or shapelet simulated galaxy sets, that is, the values of the biases and offsets are consistent with a scatter about zero bias and offset owing to the small number of galaxies in each PSF set. Even though we have assumed exponential galaxy profile the method retains its ability to fit this model to either shapelet, exponential or bulge plus disc (STEP1, that is, exponential disc plus a de Vaucouleurs bulge). This is because differences in the surface brightness profiles are subtle and not significant at low signal-to-noise ratio. The method could be extended to fit to individual nodes of substructure in galaxies with complex morphologies, and the exact form of the model profile used is not a central tenant of LENSFIT method, however since the vast majority of galaxies used in cosmic shear analysis will be faint we expect that either a de Vaucouleurs or an exponential profile will suffice.

By calculating the bias and offset as a function of size and magnitude, Figs 9 and 10, we have shown that the bias m remains at $|m| < 0.02$ over a wide range in size and magnitude. The offset c is mainly consistent with zero in the regime that there are a sufficient number of galaxies. We find a deviation from zero where the number of galaxies is very low (at bright magnitudes and large radii). The only deviations occur in the offset c where $\mathcal{M} \gtrsim 24.5$ and the size is $\mathcal{R} \lesssim 0.5$ arcsec.

We emphasize here that although this analysis has been carried out after the details of the STEP simulations were made public we did not iterate on the STEP1 or STEP2 simulations to tune any {ad hoc} parameters or vary the shape measurement method. The numerical convergence of the parameter space values were found using the zero-shear image from STEP1 PSF0. In our investigation we did however find some nuances of the STEP simulations which we will highlight. For STEP1 we found that the intrinsic ellipticity prior is very sharply peaked about zero and that the functional form used in the prior needs to be sufficiently able to fit this peak.

In STEP2, we found that to fully characterize PSFs D and E we required more stars than just the ones in the starfields. To yield an accurate PSF we co-added the PSF derived from the starfield and galaxy fields. Furthermore the PSF determined from the starfield, rotated image and unrotated image separately were not fully compatible, that is, they varied to such a degree that the shear bias and offset could be affected by up to 5 per cent if either one of the PSFs (from the starfield or galaxy images) were used individually. To resolve this issue we did re-analyse this part of data once these unexpected aspects of the simulations were found. These differences could be attributed to a number of aspects of the simulation, however we do not have sufficient information at the simulation level to make any quantitative statements in this study. The galaxy fields for PSFs A, B, C and F contained too few stars, which did not have close star–star or star–alaxy neighbours, to create a reliable additional PSF. PSFs D and E contain 30 useable stars in the galaxy images whereas the other PSFs galaxy images contain approximately 15 useable stars. Since the useable stars in the galaxy fields are also all relatively low signal-to-noise ratio this yields a noisy and unreliable PSF model from the galaxy fields for these sets. The overall conclusion, that LENSFIT yields a small bias and offset, is not dependent on this aspect of the data analysis since when PSFs

D and E are removed the method still finds a small bias and offset (Fig. 8).

An important feature of this shape measurement method is that there are no parameters which are tuned or changed in order to create an unbiased shear estimator. Originally the issue of tuning a shape measurement pipeline was raised by Bacon et al. (2001) who found that to relate measured shear to input shear a factor of 0.8 was needed for their particular KSB (Kaiser, Squires & Broadhurst 1995) implementation. Some methods, including other KSB implementations, do not require tuning parameters. However what existing shape measurement methods find, and KSB somewhat more than others, is that there are large magnitude and size dependent biases (Massey et al. 2007) and that tuning is required to eliminate these biases to some degree. Recently, Schrabback et al. (2007) and Leauthaud et al. (2007) find that they need 'shear calibration' factors of up to 0.8 so that their shear measurement pipelines agree with simulations to the 10^{-2} level over a range of magnitude.

5 AN ALTERNATIVE TO THE STEP PARAMETRIZATION

We now investigate the results going beyond the m and c parametrization. These results do not only compare the absolute values of some quantity relative to the 'ideal' result, of $m = 0$ and $c = 0$, for example, but will assess whether any deviation in the estimated shear values found by applying a shape measurement method to simulations is statistical, owing to the finite number of galaxies, or is a property of the method.

The new statistic also uses more information than the STEP parametrization. As can be seen from Fig. 4 the m and c parametrization is well suited to STEP1 in which the number of points tested in shear is small, and a linear parametrization can capture most of the relevant information. However, when using fewer galaxies per shear value (so that the variance is larger) and using many more shear values as in STEP2, the m and c parametrization disregards a large majority of the information by fitting a simple linear function through many noisy points. The approach presented here is well suited to STEP2-like simulations in which there are many shear values for which a relative large variance is expected.

5.1 The quality factor

Bridle et al. (2008) (the GRavitational lEnsing Accuracy Testing 2008, GREAT08 Handbook) define a quality factor which allows one to compare the expected statistical distribution of estimated shear values from a simulation with the distribution measured by a method. The GREAT08 quality factor is based on the work done in Amara & Refregier (2007) on the desired minimum statistical and systematic spread of estimated shear values when designing a future weak lensing survey. In this paper, we present a generalization of the GREAT08 quality factor for use in an arbitrary weak lensing simulation. The central variable used here is the same as that used in the m and c analysis, which is the difference between the estimated shear and the input shear $\gamma_i^M - \gamma_i^T$. For a good shear measurement method, that contains no biases, the variance in this quantity should be entirely statistical. The quantity used is the average mean-square error $\langle(\gamma_i^M - \gamma_i^T)^2\rangle$. The statistical spread from the simulation in question is denoted by $\sigma^2_{\rm stat}$. This expected variance is related to the measured spread of values via the 'quality factor' Q which we define as

$$Q = 1000 \frac{\sigma^2_{\rm stat}}{\frac{1}{2}\frac{1}{N_{\rm images}} \sum_{i=1,2} \sum_{\rm images} \langle(\gamma_i^M - \gamma_i^T)^2\rangle}, \quad (28)$$

where the mean-square error is averaged over γ_1 and γ_2 for each image (input shear value) in a simulation. The factor of 1000 normalizes the expression so that a method which performs well should have $Q \sim 1000$, that is, the spread in estimated shear is purely statistical. The numerator $\sigma_{\rm stat}$ is the shear variance of the galaxies analysed and is set by the simulations. The quality factor averages over all values of γ^T in an analogous way to the m and c parametrization, which fits a functional form to $\gamma_i^M - \gamma_i^T$ over all values of γ^T. This effectively averages over the angular scale on which shear is averaged as we shall discuss.

The mean square error can be written as a sum of the intrinsic variance and a bias $\langle(\gamma^M - \gamma^T)^2\rangle = \langle(\gamma^T)^2\rangle + [\text{Bias}\ (\gamma^T, \gamma^M)]^2$ where Bias $(\gamma^T, \gamma^M) = \langle\gamma^M\rangle - \gamma^T$ so that the quality factor effectively parametrizes any residual bias in the estimators γ^M; for an unbiased estimator the mean-square-error is equal to the variance of the data. This is an example of a *loss function* that parametrizes the amount that an estimator differs from an underlying distribution. The mean-square-error penalizes outliers as a result of the quadratic nature of the function, an example of a loss function that does not penalise outliers to such a degree is the absolute loss function $\langle|\gamma^M - \gamma^T|\rangle$. This loss function could also be used to make effective comparisons between the shear estimations from several different shape measurement methods, for a good shear estimator the absolute loss function should be close to zero.

When *designing* a simulation and considering what value of the quality factor would render a shape measurement method 'adequate' (for use in current or future surveys) one must define the variance in shear that a particular survey requires, σ. In Bridle et al. (2008) the numerator in the GREAT08 quality factor is effectively $10^{-4} = 1000 \times \sigma^2$ where $\sigma^2 = \sigma^2_{\rm stat} + \sigma^2_{\rm systematic}$ is the sum of expected statistical and systematic errors, and so slightly differs from the definition presented in this paper. When designing a simulation the requirement of a particular shear variance defines the number of galaxies N in the simulation via $\sigma_{\rm stat} = \sigma_\epsilon/\sqrt{N}$. This is justifiable since one can determine the shear variance that a particular survey will need in order to fully utilize the data (Van Waerbeke et al. 2006; Amara & Refregier 2007) and create a simulation that allows one to simulate the expected data.

5.2 Relation to the STEP parametrization

The relationship between the quality factor and the STEP parametrization is not straightforward and one should exercise caution when making a mapping between the two statistics, as we shall discuss. A subtlety also arises in the scale dependence of the statistics when one considers the level of bias or offset that one requires for a future survey and attempts to determine the requirement on the quality factor that this would imply.

The quality factor effectively combines, in a non-trivial but justifiable way, the information from the four STEP parameters: m, c and the uncertainties on these values Δm and Δc. As such one must take care when determining a quality factor from the absolute m and c values alone, in fitting this linear functional form, information on a method's performance is lost as a result of the assumption of the functional form itself. By using equation (24) one can relate the quality factor to the STEP m and c parametrization (for clarity in the following we let the angular brackets correspond to the averaging

over images as well as γ_1 and γ_2) the average values are calculated by integrating the function in the angular brackets over the interval $-\gamma_L$ to $+\gamma_L$ where $\gamma_L = 0.06$ in the STEP2 simulations,

$$Q = 1000\frac{\sigma^2_{\rm stat}}{\langle m^2(\gamma^T)^2 + 2cm\gamma^T + c^2\rangle} = 1000\frac{3\sigma^2_{\rm stat}}{m^2\gamma_L^2 + 3c^2}, \quad (29)$$

where we have assumed that the true shear values are evenly distributed in the range $-\gamma_L$ to $+\gamma_L$, i.e. $P(\gamma)$= constant for all $|\gamma| \leq \gamma_L$. In the case that $c = 0$ the quality factor is simply inversely proportional to m^2. This highlights the difference between the quality factor and the STEP parametrization, given a simulation the STEP parametrization quantifies a method's performance by the m and c values with the hope that $m \sim 0$, but this does not quantify whether such values achieved are statistically significant. The quality factor essentially combines the bias and offset along with the uncertainties on these values into a single parameter. As an aside we note that the substitution of the STEP parametrization into the absolute loss function gives $\langle|\gamma^M - \gamma^T|\rangle = |c|$.

As shown most recently by Fu et al. (2008, fig. 5), $\langle(\gamma^T)^2\rangle$ varies as a function of angular scale. So by choosing an average value of $\langle(\gamma^T)^2\rangle$ one implicitly assumes that m is averaged over scale. If a particular value of $\langle(\gamma^T)^2\rangle$ is chosen (as opposed to taking the average) then this corresponds to picking a certain scale over which shear variance is averaged. Furthermore a degeneracy exists when determining the required quality factor between m, c and scale. This can be seen by referring to Fu et al. (2008, fig. 5): if $c > 0$ then for a particular value of $\langle(\gamma^T)^2\rangle$ the scale to which this corresponds to will increase. The exact relation between the bias, offset and scale depends on the simulation through $\sigma_{\rm stat}$. This bias, offset and scale degeneracy highlights the fact that the quality factor itself averages over scale, but that this is no more pernicious than the STEP parametrization in this regard.

We emphasize that using the STEP m and c values to calculate a quality factor using equation (29) merely gives the maximum possible Q for those m and c values. The two panels in Fig. 11 show that for the same m and c values the quality factor can be very different (for these we assume that $\sigma^2_{\rm stat} = 10^{-7}$). From equation (29) the quality factor found using these values would be $Q = 770$, however this would only be achieved if all the points in Fig. 11 had zero scatter about the best-fitting line. The quality factor thus takes into account both the bias and offset as well as the scatter of points. However as can be seen from equation (29) different sets of m and c values can produce the same quality factor.

In the STEP2 and GREAT08 simulations $|\gamma^T| \leq 0.06$ so that $\langle(\gamma^T)^2\rangle = (1/3)(0.06)^2 \sim (0.03)^2$. If we assume that $\sigma^2_{\rm stat} \sim 10^{-7}$ and $m \sim 0.1$, as is found in STEP2 when investigating magnitude and size dependence of the methods, it can be seen that existing methods have a quality factor of $Q \lesssim 10$ which is sufficient for current surveys (see Heymans et al. 2006; and the hatched region in Fig. 5). As discussed in Bridle et al. (2008), if a method only recovers a single constant value of zero shear for any input shear value, $\gamma_1 = \gamma_2 = 0$, then $Q \sim 0.1$. When m and c values are compared with the quality factor a limit of reliability is inevitably reached since in fitting the STEP parametrization to a large number of points, as in STEP2, information on the scatter of the points is lost in the fitting process.

The issues with the quality factor that were previously discussed will only arise when designing a simulation and assessing which quality factor corresponds to a particular bias or offset requirement. When presented with existing simulations one can readily calculate the quality factor which allows the shear variance of a method to be compared to the intrinsic shear variance of the simulation.

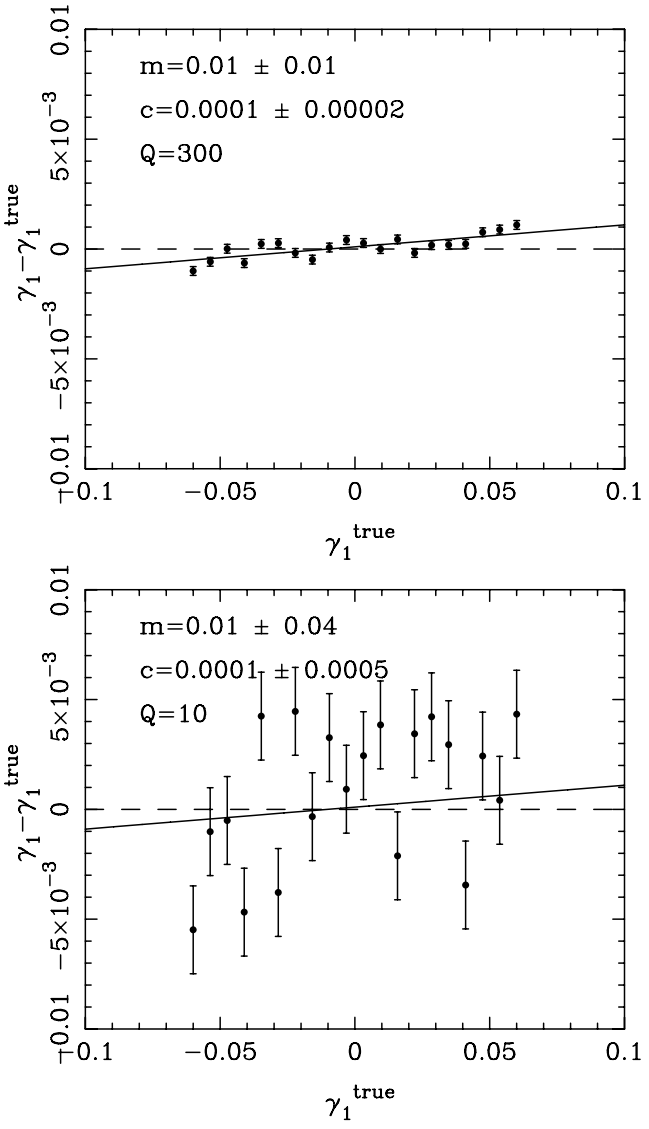

Figure 11. Simulated results of measured shear showing $\gamma^M - \gamma^T$ for two different realizations. Both panels show results which have best-fitting m and c values of $m = 0.01$ and $c = 0.0001$ the solid lines show this fit. However, the quality factor of the two results is very different owing to the scatter of points about the best-fitting line. The maximum quality factor for these m and c values would occur if all the points lay exactly on the best-fitting line, using equation (29) is $Q = 770$. In the two cases, the uncertainty on the best-fitting m and c values are different, the quality factor effectively combines the best-fitting values and the uncertainties into a single parameter.

5.3 Determination of the quality factor from the STEP2 simulation

Fig. 12 shows the spread in $\gamma_i^M - \gamma_i^T$ for γ_1 and γ_2 for the LENSFIT application to the STEP2 simulations. We do not show results for Q from STEP1 since the number of points is so small (only 5 shear values) that results on Q may be inaccurate. In Fig. 12 $c \neq 0$ would mean that the points would be scattered about a point offset from the origin, $m \neq 0$ would mean the spread of the points about zero would be larger than the intrinsic shear variance of the STEP2 simulation.

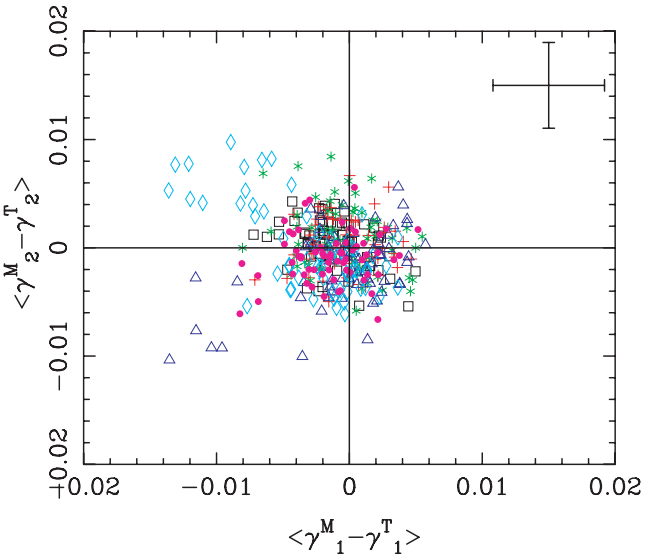

Figure 12. The values of $\gamma_1^M - \gamma_1^T$ and $\gamma_2^M - \gamma_2^T$ for all PSFs from the STEP2 simulations. The figure shows a scatter in the values about zero, the scatter is due to intrinsic variance that occurs as a result of the number of galaxies in the simulation, the scatter about zero shows that the shear offset is small. The errorbars show the average error on each point. The colours and symbols again represent the various PSFs with black (□) =PSF A, red (+)=PSF B, green (×)=PSF C, blue (△)=PSF D, cyan (◇) =PSF E, magenta (●)=PSF F.

It can be seen from Fig. 12 that there is a spread in estimated shear values about ($\gamma_1^M - \gamma_1^T \approx 0$, $\gamma_2^M - \gamma_2^T \approx 0$), that is expected for a method which can accurately estimate the shear. The points which are scattered furthest from the origin are all associated with the highly elliptical PSFs D and E. Usually the expected statistical mean-square error would be given, assuming Poisson statistics, by $\sigma^2_{\rm stat} = \langle (e_i^{\rm int})^2 \rangle / N$. However as discussed in Section 4.2 the statistical error for the STEP2 simulations is reduced due to the co-addition of rotated and unrotated images to $\sigma^2_{\rm stat} = \langle (e_i^{\rm int})^4 \rangle / 2N$ for the STEP2 simulations $\sqrt{\langle (e_i^{\rm int})^4 \rangle} \sim 0.05$ and $N \sim 3000$ so that $\sigma^2_{\rm stat} \sim 4.2 \times 10^{-7}$.

We find that for the LENSFIT application to the STEP2 simulations the global average value of $\langle (\gamma^M - \gamma^T)^2 \rangle \sim 1.1 \times 10^{-5}$ so that the global Q factor is $Q = 38$. This value shows that there is still some residual bias in the spread in the values of $\langle (\gamma_i^M - \gamma_i^T)^2 \rangle$, which we attribute to poor estimation of the prior owing to low numbers of galaxies at the extremes of magnitude and size. If the highly elliptical PSFs are removed, PSFs D and E, then the Q factor improves to $Q = 58$.

We also show how the Q value varies as a function of magnitude and size, in Table 2. When this is done the statistical variance $\sigma_{\rm stat}$ is changed since there are fewer galaxies in the corresponding bins, as shown in Table 2.

It can be seen for the variation in magnitude that the Q values are generally higher, with an average $Q \sim 150$ than for the global sample, because the prior better represents the samples intrinsic ellipticity distribution in each bin. This is the same reason that the m and c values improve in some bins when the sample is split into size and magnitude bins, as discussed in Section 4.2. There is similar variation as a function of size with an average $Q \sim 93$, the quality factor increasing as the size of the galaxies increases as one would expect since with larger galaxies the model fitting procedure becomes more reliable. The LENSFIT method therefore has an approximate quality factor of $Q \gtrsim 100$ (see Table 2) which is a factor of at least 10 times better than is required for current weak lensing surveys.

Table 2. The STEP2 quality factor Q for the global STEP2 analysis and as a function of $\mathcal{M}$ and size/radius $\mathcal{R}$, as in Table 1.

Data set	Galaxy sample	$\sigma^2_{\rm stat}$	Q
All PSFs	SExtractor matched catalogue	4.2×10^{-7}	38.5
No PSF D & E	SExtractor matched catalogue	4.2×10^{-7}	57.7
All PSFs	$18 \leq \mathcal{M} < 20$	6.3×10^{-6}	45.3
All PSFs	$20 \leq \mathcal{M} < 21$	3.2×10^{-6}	112
All PSFs	$21 \leq \mathcal{M} < 22$	1.6×10^{-6}	93.8
All PSFs	$22 \leq \mathcal{M} < 23$	1.6×10^{-6}	74.2
All PSFs	$23 \leq \mathcal{M} < 24$	6.3×10^{-6}	295
All PSFs	$24 \leq \mathcal{M} < 25$	3.1×10^{-5}	277
All PSFs	$0.2 \leq \mathcal{R} < 0.4$	3.6×10^{-7}	15.4
All PSFs	$0.4 \leq \mathcal{R} < 0.6$	7.8×10^{-7}	33.3
All PSFs	$0.6 \leq \mathcal{R} < 0.8$	1.6×10^{-6}	81.0
All PSFs	$0.8 \leq \mathcal{R} < 1.0$	3.1×10^{-6}	89.0
All PSFs	$1.0 \leq \mathcal{R} < 1.2$	1.3×10^{-5}	169

Note. STEP2 uses galaxies in the catalogues created using SExtractor and matching the rotated and unrotated catalogues.

6 CONCLUSION

In this paper, we have presented the application of the LENSFIT method of Miller et al. (2007) to simulated weak lensing data from the Shear TEsting Programme (STEP1 Heymans et al. 2006 and STEP2 Massey et al. 2007). The method is a model fitting approach to weak lensing shape measurement. The key advances over other model fitting approaches are that it uses realistic galaxy profiles and analytically integrates over the position and amplitude of the model. Furthermore we use a Bayesian shear estimation method that can take into account any bias in a fully self-contained way by using a prior ellipticity distribution. This is done by calculating a shear-sensitivity that produces a natural and correct weight function for galaxies.

In this paper, we have shown how to estimate the prior distribution from data using an iterative approach which we have shown to be stable and convergent. By using this on the STEP1 simulation we have shown that this yields a prior distribution that is a good representation of the true intrinsic ellipticity distribution. We use the model fitting method to find the full posterior probability distribution in ellipticity and then use the Bayesian approach to estimate the shear from this distribution.

This method then, yields a very small bias in the estimated shear. Furthermore it is a fast fitting method which takes approximately 1 second per galaxy (on a 2 GHz CPU) to find the full posterior probability in ellipticity and is trivially parallelizable by assigning one galaxy per CPU.

The STEP simulations parametrize the ability of a method to measure shear by fitting a linear function to the difference between the input (true) shear γ^T and the measured shear γ^M as a function of the input shear $\gamma_i^M - \gamma_i^T = m\gamma_i^T + c$. The values m and c are found which represent any bias in a method and any residual offset in the estimated shear, respectively. We have shown that LENSFIT yields values of $m = +0.006 \pm 0.005$ and $\sigma_c = 0.0002$ for the STEP1 simulations. The variance of c represents the stability of a method's estimation of shear to PSF variation. This is the smallest

combined bias and variance for any method, and the smallest bias for any method which has a linear response to the input shear.

By applying the method to the STEP2 simulations we again found that the bias $m = 0.002 \pm 0.016$ and offset $c = -0.0007 \pm 0.0006$ were very small and that the method performed very well in comparison to the methods presented in the STEP2 publication. Furthermore when the galaxy sample is split into magnitude and size bins, the bias and offset improve over a certain ranges since the intrinsic ellipticity prior varies as a function of these parameters. By recalculating the prior distribution in each bin the intrinsic distribution used is a better representation of the galaxies' true ellipticity distribution in that bin than if a global average prior is used. The bias was found to be $|m| < 0.02$ over magnitudes $20 \leq \mathcal{M} \leq 25$ and sizes of galaxy from $0.2 \leq \mathcal{R} \leq 1.2$ arcsec. The offset only deviated from $c = 0$ in the magnitude and size bins where the number of galaxies was $\ll 100$ and at the faintest magnitude and smallest sizes, for all cases the bias was $|c| \lesssim 0.004$.

The small biases we report exceed the predicted requirement for future weak lensing surveys. Amara & Refregier (2007) set a requirement for the DUNE weak lensing concept that any bias in shape measurement m needs to be be $|m| \lesssim 5 \times 10^{-3}$. Kitching et al. (2008a) present a similar required accuracy of $|m| \lesssim 8 \times 10^{-3}$ for dark energy parameters to remain unbiased. Furthermore, if the shape measurement bias is marginalized over as part of the parameter estimation then this requirement relaxes to an error on the bias of $\Delta m \lesssim 10^{-2}$. Thus we have shown in this paper that LENSFIT has the potential to negate the concern that shape measurement bias may dominate weak lensing systematics.

Going beyond the m and c parametrization we defined a quality factor Q, which quantifies whether the variation in $\gamma^M - \gamma^T$ is purely statistical, owing to the finite number of galaxies, or whether it is a result of some bias in the method. A $Q = 1000$ is where the variance is entirely statistical and $Q \sim 10$ is the limit of current methods analysed in the STEP publications. We have shown that using the STEP2 simulation that LENSFIT has a quality factor of $Q \gtrsim 100$, approximately 10 times better than is required by current surveys.

To summarize the main conclusions.

(i) Using the STEP1 simulations LENSFIT has a bias of $m \sim +6 \times 10^{-3}$ and a variation in the shear offset $\sigma_c \sim 2 \times 10^{-4}$. These are some of the smallest values for any shape measurement method.

(ii) Using the STEP2 simulations LENSFIT has a bias of $m \sim 2 \times 10^{-3}$ and a shear offset of $c \sim -7 \times 10^{-4}$, this is the smallest bias of any published method. Furthermore these values do not substantially vary when the shear values from images with highly elliptical PSF's are removed suggesting any variation is statistical.

(iii) By analysing the STEP2 simulations as function of size and magnitude the bias and offset over a certain range can improve relative to those found using the entire population as a whole. This is due to the intrinsic ellipticity prior's variation as a function of size and magnitude being correctly characterized.

(iv) We generalize the quality factor from Bridle et al. (2008) for an arbitrary simulation. Using STEP2 LENSFIT has an average $Q \gtrsim 100$, when the prior is correctly calculated in each magnitude or size bin, which is at least a factor of 10 times larger than current methods and the accuracy required by existing surveys.

In a real survey, there are a number of sophistications which the STEP simulations do not include. None of these should present an insurmountable problem to this method. The PSF will vary as a function of position, but given a large enough number of stars in each region this can be determined. Currently, we reject any close pairs of galaxies when two or more galaxies lie in the same postage stamp, this could be improved so that for pairs in which there is one high signal-to-noise ratio galaxy and one very low signal-to-noise galaxy the pair is kept, or adaptive postage stamp sizes could be used. In cases of multiple exposures the posterior probability for each galaxy and each exposure may be combined in an optimal way. In other respects the STEP simulations are more difficult to analyse using this method than in a real survey, for example our assumption that the prior intrinsic ellipticity distribution is centred on zero is not true in the STEP simulations since the ellipticity is constant across the whole image. In reality, where the mean shear across an image should be zero, the assumption of a zero-centred prior should be a good representation of this distribution.

The LENSFIT method outperforms the majority of other shape measurement methods since it uses realistic galaxy profiles and crucially uses a Bayesian method to remove bias. We have shown that the method reaches a level of accuracy, on simulated data sets, that surpasses the level which current surveys require. This gives us confidence that future weak lensing surveys which use such a technique will not be limited by the ability to measure the shapes of galaxies.

ACKNOWLEDGMENTS

TDK is supported by the Science and Technology Facilities Council, research grant number E001114. CH is supported by the European Commission Programme in the framework of the Marie Curie Fellowship under contract MOIF-CT-2006-21891. We thank Richard Massey and the STEP collaboration for making the STEP simulations publicly available. We thank Adam Amara, Sarah Bridle, Konrad Kuijken, Alexandre Refregier and all members of the GREAT08 team for insightful discussions.

REFERENCES

Albrecht A., 2006, Report of the Dark Energy Task Force, preprint (astro-ph/0609591)
Amara A., Refregier A., 2007, 381, 3
Bacon D. J., Taylor A. N., 2003, MNRAS, 344, 1307
Bacon D. J., Refregier A., Clowe D., Ellis R. S., 2001, MNRAS, 325, 1065
Benjamin J. et al., 2007, MNRAS, 381, 702
Bernstein G. M., Jarvis M., 2002, AJ, 123, 583
Bertin E., Arnouts S., 1996, A&AS, 117, 393
Bridle S., Kneib J.-P., Bardeau S., Gull S., 2002, in Priyamvada Natarajan, ed., Proc. Yale Cosmology Workshop, The Shapes of Galaxies and Their Dark Matter Halos. World Scientific, Singapore
Bridle S. et al., 2008, GRavitational lEnsing Accuracy Testing Handbook
Crittenden R., Natarajan P., Pen U., Theuns T., 2001, AJ, 559, 552
Dunlop J. S., McLure R. J., Kukula M. J., Baum S. A., O'Dea C. P., Hughes D. H., 2003, MNRAS, 340, 1095
Fu L. et al., 2008, A&A, 474, 4
Heavens A., 2003, MNRAS, 343, 1327
Heavens A. F., Kitching T. D., Taylor A. N., 2006, MNRAS, 373, 105
Heymans C. et al., 2006, MNRAS, 368, 1323
Hu W., 1999, ApJ, 522, 21
Jarvis M., Jain B., 2005, preprint (astro-ph/0412234)
Jee M. J., Blakeslee J. P., Sirianni M., Martel A. R., White R. L., Ford H. C., 2008, PASP, 114, 1403
Kaiser N., 2000, ApJ, 537, 555
Kaiser N., Squires G., Broadhurst T., 1995, ApJ, 449, 460
Kaiser N. et al., 2002, Proc. SPIE Vol. 4836, p. 154, 4836, 154
Kim A. et al., 2002, Proc. SPIE Vol. 4836, p. 154, 4836, 53

Kitching T. D., Heavens A. F., Taylor A. N., Brown M. L., Meisenheimer K., Wolf C., Gray M. E., Bacon D. J., 2007, MNRAS, 376, 771
Kitching T. D., Heavens A. F., Taylor A. N. 2008, MNRAS, submitted (astro-ph arXiv:0801.3270)
Kuijken K., 1999, A&A, 352, 355
Kuijken K., 2006, A&A, 456, 827
Leauthaud A. et al., 2007, ApJS, 172, 219
Lucy L., 1974, AJ, 79, 745
Lucy L., 1994, A&A, 289, 983
Luppino G. A., Kaiser N., 1997, ApJ, 475, 20
Massey R., Refregier A., Conselice C., Bacon D., 2004, MNRAS, 348, 214
Massey R., Refregier A., 2005, MNRAS, 363, 197
Massey R., Rowe B., Refregier A., Bacon D. J., Berge J., 2007a, MNRAS, 380, 229
Massey R. et al., 2007b, MNRAS, 376, 13
Miller L., Kitching T. D., Heymans C., Heavens A. F., Van Waerbeke L., 2007, MNRAS, 382, 31
Munshi D., Valageas P., Van Waerbeke L., Heavens A., 2007, preprint (arXiv:astro-ph/0612667)
Paulin-Henriksson S., Amara A., Voigt L., Refregier A., Bridle S. L., 2008, A&A, 484, 67
Peacock J., Schneider P., Efstathiou G., Ellis J. R., Leibundgut B., Lilly S. J., Meller Y., 2006, Report by the ESA–ESO working group on fundamental cosmology, ESA Publications Division, Noordwijk (astro-ph/0610906), preprint (eprint arXiv:astro-ph/0610906)
Refregier A., 2003, MNRAS, 338, 35
Refregier A., Bacon D., 2003, MNRAS, 338, 48
Refregier A. et al., 2006, Proc. SPIE Vol. 4836, p. 154, 6265, 58
Richardson W. H., 1972, J. Opt. Soc. Am., 62, 55
Schrabback T. et al., 2007, A&A, 468, 823
Seitz C., Schneider P., 1997, A&A, 318, 687
Spergel D. et al., 2007, ApJS, 170, 377
Taylor A. N., Kitching T. D., Bacon D. J., Heavens A. F., 2007, MNRAS, 374, 1377
Tyson J. A., Wittman D. M., Hennawi J. F., Spergel D. N., 2003, Nucl. Phys. B, 124, 21
Van Waerbeke L., White M., Hoekstra H., Heymans C., 2006, Astropart. Phys. 26, 91101

This paper has been typeset from a TEX/LATEX file prepared by the author.